Chapter 17
Radiation Damage

17.1 INTRODUCTION

The preceding chapters have dealt with some of the observable consequences of fission-fragment irradiation of ceramic fuel materials; succeeding chapters will be concerned with changes in the properties of cladding metals resulting from fast-neutron bombardment. These macroscopic, observable, and often technologically crucial results of exposure of solids to energetic particles are collectively known as *radiation effects*. The primary, microscopic events that precede the appearance of gross changes in the solid are termed *radiation damage*. This branch of physics attempts to predict the number and configuration of the point defects (vacancies and interstitial atoms) produced by the bombarding particles. Radiation-damage analyses are not concerned with what the defects go on to do in the solid—such processes are properly categorized as radiation effects. Radiation damage and radiation effects can also be distinguished by their characteristic time scales; the primary events produced by nuclear irradiation are over in less than 10^{-11} sec after the bombarding particle has interacted with the solid. Subsequent processes require much longer times; the diffusion of radiation-produced point defects to sinks in the solid can take milliseconds. The time scale of the nucleation and growth of voids in metals by agglomeration of radiation-produced vacancies is of the order of months.

The primitive damage-producing processes involve the interaction of lattice atoms with particles possessing energies far in excess of thermal energy ($\sim$kT). Consequently, the temperature of the solid is of no importance in the analysis of radiation damage. The processes included under radiation effects, however, are concerned with point defects, or clusters thereof, which are in thermal equilibrium with the host crystal. The kinetics of such processes are therefore highly dependent on solid temperature, which invariably appears as a Boltzmann factor, exp (−E/kT), where E is the characteristic energy of a thermodynamic process or a migratory event.

The energy transferred to a stationary lattice atom in a collision with a high-energy bombarding particle is of the order of tens to hundreds of kiloelectron volts. This quantity of energy is so much larger than the energy binding the atom in its lattice site that displacement of the struck atom is virtually certain. The lattice atom first struck and displaced by the bombarding particle is called the *primary knock-on atom*, or PKA. Because a PKA possesses substantial kinetic energy, it becomes an energetic particle in its own right and is capable of creating additional lattice displacements. These subsequent generations of displaced lattice atoms are known as *higher order knock-ons*, or *recoil atoms*. An atom is considered to have been displaced if it comes to rest sufficiently far from its original lattice site that it cannot return spontaneously. It must also be outside the recombination region of any other vacancy created in the process. The displaced atom ultimately appears in the lattice as an interstitial atom. The empty lattice sites left behind by the displaced atoms (equal in number to the displaced atoms) are indistinguishable from ordinary thermally produced vacancies. The ensemble of point defects created by a single primary knock-on atom is known as a *displacement cascade*.

The earliest and simplest theory of radiation damage treated the cascade as a collection of isolated vacancies and interstitials and gave no consideration to the spatial distribution of the point defects. In the crudest approximation the number of displaced atoms is computed by approximating the collision partners as hard spheres; the only physical property of the solid needed in this model is the energy that a lattice atom must acquire in a collision in order to be displaced. Many improvements on this simple collision model have been made, but the idea of a cascade consisting of isolated point defects has been retained. Hard-sphere scattering can be replaced by energy-transfer cross sections based on realistic interatomic potentials. The loss of energy of a moving atom by interaction with the electrons of the medium, in addition to elastic collisions between atoms, can be added to simple cascade theory. Finally, the simple model can be improved by considering energy-loss mechanisms peculiar to the periodicity of the crystalline lattice, the most important of which are focusing and channeling.

Radiation damage is not restricted to the isolated point defects produced by the bombarding particles. Indeed, vacancies and interstitials can be produced so close to each other that clustering of the point defects occurs spontaneously within the short time required for completion of the primary event. When the distance between successive collisions of a recoil atom and the stationary lattice atoms approaches the interatomic spacing of the crystal structure,

it is clearly inappropriate to model the cascade as a collection of isolated vacancies and interstitials. Instead, a dense cluster of point defects called a *displacement spike* or *depleted zone* is formed. Because of the proximity of the point defects in a displacement spike, the probability of near-instantaneous annihilation of many of the vacancies and interstitials produced by the high-energy collisions becomes large. In fact, the number of point defects that actually survive a cascade and are capable of producing observable radiation effects can be as low as 1% of the number predicted by simple cascade theory.

The cascade is initiated by a primary knock-on atom. The cascade therefore consists of many interactions between moving and stationary atoms of the same kind. The primary knock-on atom, on the other hand, is produced by a bombarding particle arising directly from some nuclear event, principally the fission process. In terms of damage-producing capabilities, the most important nuclear particles are the fission fragments (in fuel materials) and fast neutrons (in the cladding and structural materials). Other energetic subatomic particles, such as electrons, protons, alpha particles, and gamma rays, can also initiate displacement cascades. However, these particles are either far less damaging than fission fragments (e^- and γ) or are produced in such small quantities in reactor fuel elements that their contribution to the total damage is negligible (p and α). Only fast neutrons and fission fragments are considered as bombarding particles in this chapter, and only the theoretical treatment of radiation damage in monatomic solids will be reviewed. For practical purposes of estimating damage in reactor materials, the calculations for elemental solids are usually simply applied without modification to multielement systems, such as the fuel $(U,Pu)O_2$ or the alloy stainless steel.

To calculate the displacement rate, we must know the total flux and the energy spectrum of the bombarding particles. For fast neutrons the differential flux, $\phi(E_n)$, is obtained from reactor-physics calculations. The equivalent quantity for fission fragments can be obtained from the fission density, $\dot{F}$, and a reasonable assumption concerning the energy loss of the fragments in the fuel. If the energy spectrum of the flux of bombarding particles and the energy-transfer cross section for collisions between these particles and atoms of the lattice are known, the number of primary knock-on atoms in a differential energy range can be computed. The final step is to use this source spectrum of the primary knock-on atoms to determine the total number of recoils, or displaced atoms, using cascade theory. Such a computation provides the best available estimate of the damage inflicted on a solid by irradiation for those properties which depend primarily on the presence of isolated point defects (e.g., irradiation creep and void growth). On the other hand, when such forms of damage as irradiation hardening or embrittlement are of interest, the size and number density of displacement spikes are more important than the concentration of isolated vacancies and interstitials that have escaped from the spike. In this instance, analytic cascade theories that predict only the number of displaced atoms, no matter how sophisticated from the point of view of atomic collisions, are not germane. The characteristics of the clusters of defects created by a PKA can best be ascertained by computer simulation of the radiation-damage process.

To predict either the number of displaced atoms by an analytical isolated point-defect cascade model or to compute the configuration of a displacement spike by a computer experiment requires that the interatomic potential between atoms of the solid be known. A great deal of information on atomic interaction potentials has been obtained by analysis of the equilibrium properties of a solid (Chap. 4). Unfortunately, these potential functions represent the interaction at separation distances of the order of a lattice constant, whereas the potential at much smaller separations is relevant in radiation-damage calculations, which involve much higher particle energies. For very high energies the colliding atoms approach each other so closely that the bare nuclei interact in a manner prescribed by a Coulomb potential. In the energy range characterizing most of the collisions responsible for cascade production, however, the nuclear charges are partially screened by the atomic electrons, and no completely satisfactory interatomic potential describes the interaction. The screened Coulomb potential (sometimes called the Bohr potential), the inverse power law potential, and the Born–Mayer potential are frequently used. Because of the computational difficulties involved in dealing with potential functions that lead to nonisotropic scattering in the center-of-mass system, these potentials are often used only to compute the radius of the equivalent hard sphere characterizing the collision, but the collision dynamics are determined from the hard-sphere model (which gives isotropic scattering in center-of-mass coordinates). In radiation-damage calculations only the repulsive portion of the interatomic potential function is needed. The attractive forces between lattice atoms, which are important in the equilibrium properties of the solid, play no part in the events associated with radiation damage.

The interaction between a moving atom and the lattice atoms is almost universally treated as a sequence of two-body elastic collisions. The binary-collision assumption is quite satisfactory at high interaction energies because the approach distances giving substantial energy transfer are very much smaller than the distances between lattice atoms; thus the collisions can be considered to occur between isolated pairs of atoms. At energies approaching the threshold energy for displacement, however, the cross section for atom–atom interaction is large, and the incoming atom can interact with more than one atom at the same time.

The collision between a recoil and a lattice atom is often assumed to be elastic, which means that kinetic energy is conserved in the event. Inelasticity can arise from excitation or ionization of the orbital electrons of the atoms involved in the collision. Indeed, interaction of moving atoms or ions with the electrons of the solid constitute the major energy-loss process at high energies. Transfer of energy from the moving atom to electrons does not lead to displacement, only to heat; the low electron mass means that they carry little momentum even though they may be quite energetic. Consequently, it is important to be able to estimate the degree to which the energy of a recoil atom is partitioned between electronic excitation and

elastic atom–atom collisions. Only the energy transferred in the latter process is available for causing displacements. Energy is transferred to the electrons in small increments so closely spaced that the process can be regarded as a continuous loss of energy by the moving atom. The atom continues to travel in a straight line but slows down as if it were passing through a viscous medium. The atom–atom interactions, on the other hand, occur at widely spaced intervals, transfer a significant portion of the initial kinetic energy of the moving atom in an essentially instantaneous collision, and produce substantial deflections of the original energetic atom. Consequently, the total energy loss of a moving atom can be accurately separated into two parts: (1) discrete elastic atom–atom encounters which both reduce the energy of the incident atom and produce lattice displacements and (2) a continuous process of electronic excitation which contributes to energy loss but not to displacements.

Not all the energy transferred to a stationary lattice atom by a recoil atom by process 1 is used to displace the former. A substantial portion of the initial energy of the PKA is degraded to heat by atom–atom collisions that do not deliver the requisite displacement energy to the struck atom. In this event the struck atom simply rattles about in its lattice site, ultimately degrading the energy it received in the collision to heat.

There are several excellent books dealing with the subject of radiation damage in a comprehensive and detailed manner.[1-6] In this chapter only those aspects of the theory pertinent to the performance of nuclear fuel elements are considered. Details of some derivations have been omitted when they can be found in one of the books devoted solely to the field of radiation damage.

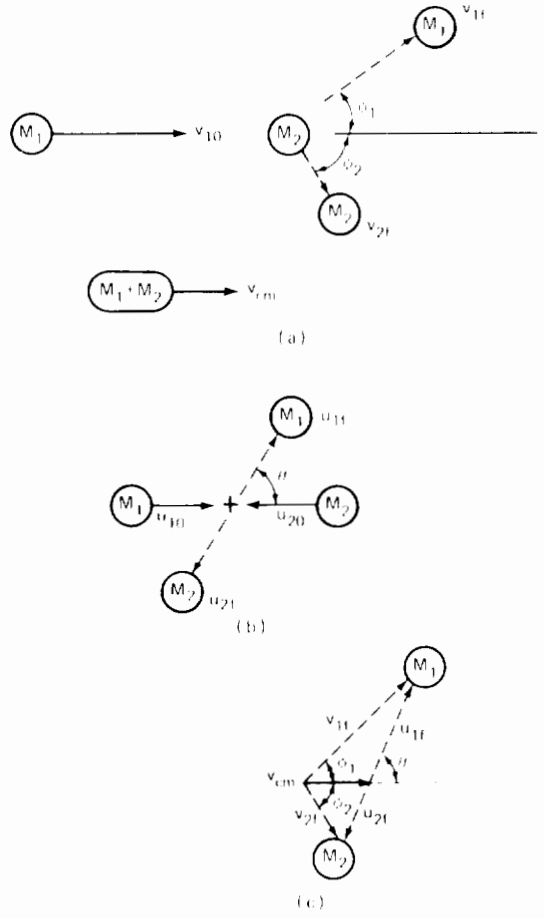

Fig. 17.1 Binary collision between a projectile of mass M_1 and a target particle of mass M_2. (a) Laboratory frame of reference. (b) Center-of-mass coordinates. (c) Vector diagram relating the velocities in the two coordinate systems.

17.2 BINARY ELASTIC-COLLISION DYNAMICS

17.2.1 Scattering Angles and Energy Transfer

Many useful aspects of binary collisions can be obtained without knowledge of the interatomic potential by application of the laws of momentum and energy conservation. Only nonrelativistic elastic collisions are considered. The masses of the interacting particles are denoted by M_1 and M_2. Particle 1 (the projectile) approaches stationary particle 2 (the target) with speed v_{10}. Figure 17.1(a) shows the speeds and directions of the particles before and after the collision in the laboratory frame of reference, which is at rest with respect to the observer. The analysis is simplified by transforming the coordinates from the laboratory system to one that moves with the velocity of the center of mass of the two-particle system. The speed of the center of mass is given by

$$v_{cm} = \left(\frac{M_1}{M_1 + M_2}\right) v_{10} \tag{17.1}$$

Since the center-of-mass velocity is unchanged by the collision, the event appears in the new coordinate system as shown in Fig. 17.1(b). The initial speeds of the particles in the center-of-mass system are related to those in the laboratory system by

$$u_{10} = v_{10} - v_{cm} \tag{17.2a}$$

$$u_{20} = v_{cm} \tag{17.2b}$$

The direction of u_{20} is opposite to that of u_{10}. The scattering angle in the center-of-mass system is θ.

When the collision is viewed in the center-of-mass system, the recoiling particles appear to move away from each other in opposite directions. Momentum conservation along the axes of approach and departure yield

$$M_1 u_{10} + M_2 u_{20} = M_1 u_{1f} + M_2 u_{2f} \tag{17.3}$$

and conservation of kinetic energy requires that

$$\frac{1}{2} M_1 u_{10}^2 + \frac{1}{2} M_2 u_{20}^2 = \frac{1}{2} M_1 u_{1f}^2 + \frac{1}{2} M_2 u_{2f}^2 \tag{17.4}$$

Equations 17.3 and 17.4 are satisfied only if

$$u_{1f} = u_{10} = v_{10} - v_{cm} \tag{17.5a}$$

$$u_{2f} = u_{20} = v_{cm} \tag{17.5b}$$

The particle velocities in the laboratory system after the collision are determined by vectorially adding the center-of-mass velocity to u_{1f} and u_{2f}, or

$$v_{1f} = u_{1f} + v_{cm} \tag{17.6a}$$

$$v_{2f} = u_{2f} + v_{cm} \tag{17.6b}$$

The magnitudes of v_{1f} and v_{2f} can be obtained from the vector diagrams shown in Fig. 17.1(c). Application of the law of cosines to the lower diagram yields

$$\begin{aligned} v_{2f}^2 &= v_{cm}^2 + u_{2f}^2 - 2v_{cm}u_{2f}\cos\theta \\ &= 2v_{cm}^2(1-\cos\theta) \end{aligned} \tag{17.7}$$

where u_{2f} was expressed by Eq. 17.5b in order to arrive at the second equality in the above equation. We can eliminate v_{cm} from Eq. 17.7 by using Eq. 17.1, which produces

$$v_{2f}^2 = \frac{2M_1^2 v_{10}^2}{(M_1+M_2)^2}(1-\cos\theta)$$

Noting that $E_{10} = M_1 v_{10}^2/2$ is the kinetic energy of the projectile and $E_{2f} = M_2 v_{2f}^2/2$ is the kinetic energy of the recoil particle, we can write the above formula

$$E_{2f} = \frac{2M_1M_2}{(M_1+M_2)^2}E_{10}(1-\cos\theta)$$

To simplify this notation for subsequent use, we replace E_{10} by E and denote E_{2f} by T, the energy transferred to the struck particle by the collision. The group containing the mass numbers is given a special symbol:

$$\Lambda = \frac{4M_1M_2}{(M_1+M_2)^2} \tag{17.8}$$

and the energy-transfer equation becomes

$$T = \frac{1}{2}\Lambda E(1-\cos\theta) \tag{17.9}$$

The maximum possible energy transferred from the moving particle to the stationary one occurs in a head-on collision, for which $\theta = \pi$ and

$$T_m = \Lambda E \tag{17.10}$$

If the particles are identical, $\Lambda = 1$, and any energy between 0 and E can be transferred in the collision.

The scattering angle in the laboratory system, ϕ_1, and the direction of the struck atom after the collision, ϕ_2, can be related to the scattering angle in the center-of-mass system with the aid of the vector diagram of Fig. 17.1(c). Applying the law of sines to the triangle representing the scattered projectile yields

$$\frac{v_{1f}}{\sin(\pi-\theta)} = \frac{u_{1f}}{\sin\phi_1}$$

where u_{1f} is given by Eq. 17.5(a), from which v_{cm} can be eliminated by Eq. 17.1, giving

$$u_{1f} = v_{cm}\left(\frac{v_{10}}{v_{cm}} - 1\right) = v_{cm}\frac{M_2}{M_1}$$

Applying the law of cosines to the same triangle yields

$$v_{1f}^2 = u_{1f}^2 + v_{cm}^2 - 2v_{cm}u_{1f}\cos(\pi-\theta)$$

Combining these three equations and rearranging yields

$$\tan\phi_1 = \frac{(M_2/M_1)\sin\theta}{1+(M_2/M_1)\cos\theta} \tag{17.11a}$$

Similarly, the law of sines for the vector diagram for the recoil particle yields

$$\frac{u_{2f}}{\sin\phi_2} = \frac{v_{2f}}{\sin\theta}$$

which, when combined with Eqs. 17.5b and 17.7, results in the relation

$$\tan\phi_2 = \frac{\sin\theta}{1-\cos\theta} \tag{17.11b}$$

17.2.2 Some Properties of the Head-On Collision

The preceding analysis is valid for any nonrelativistic elastic collision for any center-of-mass scattering angle θ provided the collision partners in the initial and final states are sufficiently far apart that the interaction energy between them is negligible compared to their kinetic energies. During the collision event, however, the separation distance is small, and the conversion of kinetic energy to potential energy is important. In particular, for a head-on collision ($\theta = \pi$), the kinetic energy (exclusive of the kinetic energy of the center of mass) becomes zero at the point where the particles turn around and begin to retrace their paths. During a head-on collision, momentum conservation can be expressed by

$$v_{cm} = \left(\frac{M_1}{M_1+M_2}\right)v_1 + \left(\frac{M_2}{M_1+M_2}\right)v_2$$

where v_1 and v_2 are the laboratory-system speeds of the two particles at some point during the collision. The relative speed of the two particles is defined by*

$$g = v_1 - v_2 \tag{17.12}$$

Rearrangement of the above two formulas permits v_1 and v_2 to be expressed as functions of v_{cm} and g:

$$v_1 = v_{cm} + \left(\frac{M_2}{M_1+M_2}\right)g \tag{17.13a}$$

$$v_2 = v_{cm} - \left(\frac{M_1}{M_1+M_2}\right)g \tag{17.13b}$$

The total kinetic energy of the two particles is given by

$$KE = \frac{1}{2}M_1v_1^2 + \frac{1}{2}M_2v_2^2$$

or, when expressed in terms of v_{cm} and g, by

$$KE = \frac{1}{2}(M_1+M_2)v_{cm}^2 + \frac{1}{2}\mu g^2$$

*In the general elastic collision treated in Sec. 17.2.1, the initial and final relative speeds g_0 and g_f are represented by the distances separating the two particles in the diagram of Fig. 17.1(b) before and after the collision. The values of g_0 and g_f have the same magnitude; the collision simply rotates the relative velocity vector by an angle θ.

where

$$\mu = \frac{M_1 M_2}{M_1 + M_2} \tag{17.14}$$

is the reduced mass of the system. Thus, the total kinetic energy can be divided into two parts, one due to the motion of the system as a whole described by v_{cm} and the other arising from the relative kinetic energy of the two particles. The latter is

$$E_r = \frac{1}{2}\mu g^2 \tag{17.15}$$

During the collision the kinetic energy of the center of mass is unchanged, but the relative kinetic energy decreases as the potential energy becomes significant, which occurs at close separation distances. Conservation of total energy at any point in the collision requires that

$$E_r + V(x) = E_{r0} \tag{17.16}$$

where $V(x)$ is the potential energy of interaction at a head-on separation distance x and E_{r0} is the relative kinetic energy in the initial state, which is taken to be at infinite separation. An important special case of Eq. 17.16 occurs at the distance of closest approach, x_m, where the relative kinetic energy is zero. If the collision partners are of the same mass, $\mu = M/2$, and if the target atom is initially at rest, $g_0 = v_{10}$, Eq. 17.16 then reduces to

$$V(x_m) = \frac{E}{2} \tag{17.17}$$

where $E = M_1 v_{10}^2/2$ is the kinetic energy of the projectile. This formula will be used to deduce equivalent hard-sphere radii as a function of energy for particular types of interatomic potential functions.

17.3 BASIC CONCEPTS

The terminology pertinent to the collision and energy-loss processes involving large numbers of energetic atoms in a solid is reviewed in this section.

17.3.1 Cross Section

The primitive idea of a cross section is shown in Fig. 17.2. Consider a single projectile (or bombarding particle) passing through a medium consisting of N target particles per unit volume. Target species are assumed to be distributed randomly. We wish to formulate the probability that the projectile collides with a target particle while traversing a path length dx in the medium. If the incident particle strikes the front face of the dx-thick slice within any one of the projected areas, σ, characterizing the target particles, a collision occurs. The volume element in the drawing contains N dx particles whose projected areas occupy a fraction σN dx of the front face of the volume element. The chance of an interaction is therefore:

$N\,\sigma(E)\,dx$ = Probability of the collision of an incident particle with a target particle in dx (17.18)

Equation 17.18 defines the *total collision cross section* between the incident and target species when the energy of the former is E. The total cross section is a measure of the probability of occurrence of any type of collision between the two particles. Cross sections of more restricted types of interactions can be similarly defined. For example, we may require that the collision transfer energy between T and T + dT to the target particle during the collision and define the *differential energy-transfer cross section* by:

$N\,\sigma(E,T)\,dT\,dx$ = Probability of a collision in the distance dx which transfers energy in the range (T,dT) to the target particle (17.19)

The differential and total cross sections are related by

$$\sigma(E) = \int_0^{T_m} \sigma(E,T)\,dT \tag{17.20}$$

where T_m is the maximum energy transferable in a collision. For elastic collisions, T_m is given by Eq. 17.10.

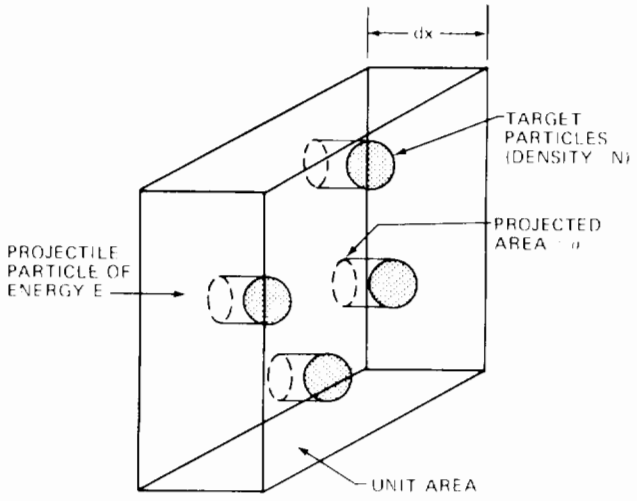

Fig. 17.2 The collision cross section.

The *differential angular cross section* describes the probability of an interaction that results in deflection of the incident particle by an angle θ in the center-of-mass system:

$N\,\sigma(E,\theta)\,d\Omega\,dx$ = Probability of a collision in dx which scatters the incident particle into a center-of-mass angle in the range $(\theta, d\Omega)$ (17.21)

where $d\Omega$ is an element of solid angle about the scattering direction θ. Inasmuch as scattering is azimuthally symmetric (i.e., equally probable in any direction in the plane perpendicular to the x-direction in Fig. 17.2), the solid-angle increment is

$$d\Omega = 2\pi\, d(\cos\theta)$$

For elastic scattering, Eq. 17.9 provides a unique relation between T and θ; thus the angular and energy-transfer differential cross sections are connected by

$$2\pi\,\sigma(E,\theta)\,d(\cos\theta) = \sigma(E,T)\,dT$$

or

$$\sigma(E,T) = 2\pi\,\sigma[E,\theta(T)]\left|\frac{d(\cos\theta)}{dT}\right| = \left(\frac{4\pi}{\Delta E}\right)\sigma[E,\theta(T)] \qquad (17.22)$$

The ratio of the differential elements $d(\cos\theta)$ and dT is obtained from Eq. 17.9. The second equality in Eq. 17.22 contains this transformation. The notation $\theta(T)$ means that θ is expressed as a function of T using the same equation. Equation 17.22 permits the differential energy-transfer cross section to be determined if the differential angular cross section is known. When scattering is isotropic in the center-of-mass system, $\sigma[E,\theta(T)] = \sigma(E)/4\pi$.

17.3.2 Mean Free Path

The *mean free path* is the average distance travelled by an incident particle between collisions. Equation 17.18 shows that the number of collisions per unit path length is $N\sigma(E)$. The reciprocal of this quantity is the average path length per collision, or

$$l(E) = \frac{1}{N\sigma(E)} = \text{Mean free path of a particle of energy E} \qquad (17.23)$$

17.3.3 Current and Flux

The *current* describes the rate of transport of particles if they are all travelling in one direction, and the *flux* is the analogous measure for particles that are moving in many different directions.

The total current is defined by

$$I = \text{Number of particles crossing a plane of unit area perpendicular to the particle direction per second} \qquad (17.24)$$

When the particles are not moving in a single direction, the flux is defined in terms of the unit sphere:

$$\Phi = \text{Number of particles crossing a sphere of unit projected area per second} \qquad (17.25)$$

The flux can be restricted to those particles within the energy range from E to E + dE:

$$\phi(E)\,dE = \text{Number of particles with energies in the range (E,dE) crossing the unit sphere per second} \qquad (17.26)$$

where $\phi(E)$ is the differential energy flux, or simply the differential flux or the energy flux and is related to the total flux by

$$\Phi = \int_0^\infty \phi(E)\,dE \qquad (17.27)$$

17.3.4 Collision Density

If the current of incident particles entering the volume element in Fig. 17.2 is I and if each particle has a probability given by Eq. 17.18 of interacting, the number of collisions per unit volume per second is $NI\sigma$. This expression can be generalized to describe the collision rate in a flux spectrum for interactions that transfer energy in a particular range. Thus

$$F(E,T)\,dE\,dT = \text{Collisions per unit volume per unit time between target particles and incident particles in the range (E,dE) which result in energy transfer to the target particle in the range (T,dT)} = N\phi(E)\,\sigma(E,T)\,dE\,dT \qquad (17.28)$$

Equation 17.28 can also be regarded as a source term expressing the volumetric rate of production of the recoils in the energy range (T,dT):

$$N\left[\int_0^\infty \phi(E)\,\sigma(E,T)\,dE\right]dT = \text{Number of recoil atoms produced per unit volume per unit time with energies in the range (T,dT)}$$

17.3.5 Stopping Power and Range

The *stopping power* is the energy lost by a moving particle per unit of length travelled in the medium. Equation 17.19 gives the probability of a collision in path length dx which results in energy loss between T and T + dT. The average energy loss in dx is obtained by multiplying Eq. 17.19 by the energy transfer T and integrating over all possible values of T:

$$\langle dE\rangle = N\int_{T_0}^{T_m} T\,\sigma(E,T)\,dT\,dx = \text{Average energy loss of a particle of energy E in moving a distance dx}$$

Dividing this equation by dx and omitting the averaging symbol on dE gives the stopping power:

$$\frac{dE}{dx} = N\int_{T_0}^{T_m} T\,\sigma(E,T)\,dT \qquad (17.29)$$

The minimum energy transferred, T_0, need not be zero. The stopping cross section is defined as

$$\frac{1}{N}\frac{dE}{dx} = \int_{T_0}^{T_m} T\,\sigma(E,T)\,dT \qquad (17.29a)$$

The *range* is a measure of the path length in the solid traversed by a particle from the point of its birth in or entry into the solid to the point at which it no longer possesses kinetic energy. Two ranges can be defined: one easy to calculate and the other easy to measure. Figure 17.3 shows a typical history of a particle that makes a number of collisions before it is stopped. The arrows indicate the path length between successive collisions. They are approxi-

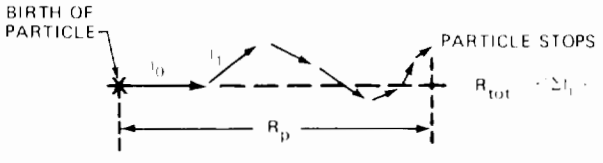

Fig. 17.3 Path of a typical particle slowing down in a solid showing the mean and projected ranges.

mately equal to the mean free path. The total range is defined as the mean value of the sum of the linear segments between collisions between birth and stopping of the particle:

$$R_{tot} = \langle \Sigma l_i \rangle$$

The total range is related to the stopping power by

$$R_{tot}(E) = \int_0^{R_{tot}(E)} dx = \int_0^E \frac{dE'}{(dE'/dx)} \qquad (17.30)$$

The total range can be computed if the dependence of the stopping power on energy is known. According to Eq. 17.29 the differential energy-transfer cross section is needed for this calculation.

The projected range, R_p, is the component of the total range along the initial direction of the particle. For an interatomic potential that varies as the inverse square of the separation distance, the two ranges are related by:[7]

$$\frac{R_{tot}}{R_p} = 1 + \frac{1}{3}\left(\frac{M_2}{M_1}\right) \qquad (17.31)$$

where M_2 and M_1 are the masses of the target and projectile species, respectively. Although R_p is always less than R_{tot}, the difference between the two ranges is reduced as the average energy transferred per collision becomes smaller (i.e., for $M_2/M_1 \gg 1$).

The concepts of stopping power and range are most useful when many small-energy-transfer collisions occur during particle slowing down. In this case the energy loss process is nearly continuous, and the deflection per collision is also small. The interaction of atomic particles with the electrons of a solid is an example of this type of slowing down. The maximum energy transferred to an electron by a particle of mass M is a fraction, $4m_e/M \sim 0.002/M$, of the kinetic energy of the moving atom, and, according to Eq. 17.11a, the deflection angle per collision is $m_e/M \sim 10^{-5}$ radians.

17.4 POTENTIAL FUNCTIONS AND ENERGY-TRANSFER CROSS SECTIONS

The manner in which the potential energy of a two-particle system varies with the distance separating the two centers determines both the equilibrium properties of an assembly of atoms and the way that energetic particles interact with a lattice of stationary atoms. The relation between the interatomic potential function and the equilibrium properties of the solid is discussed in Chap. 4. The potential function appears in radiation-damage theory via the differential energy-transfer cross section, $\sigma(E,T)$, which determines the energy loss rates, the collision density, the mean free path, and other properties of the slowing-down process. The differential energy-transfer cross section is uniquely determined by the potential function, although the connection between $V(r)$ and $\sigma(E,T)$ is rather complex. Only a few simple potential functions can be converted to analytical expressions for the differential cross section.

17.4.1 Potential Functions

Because no single potential function applies over the entire range of separation distances between atoms or ions, it is useful to consider the limiting cases of very-high-energy collisions (small distances of approach) and near-thermal energies (i.e., tens of electron volts) where the electronic clouds of the two species just begin to overlap. There are two principal contributions to the repulsive potential between two atoms which correspond to these extremes: (1) the electrostatic repulsion between the positively charged nuclei and (2) the increase in energy required to maintain the electrons of nearby atoms in the same region of space without violating the Pauli exclusion principle. Since no two electrons can occupy the same position, overlapping of electrons from two atoms must be accompanied by promotion of some of the electrons to higher, unoccupied levels of the atomic structure. The energy required for this process increases as the atoms approach each other because a larger number of the orbital electrons become affected.

At separations somewhat smaller than the equilibrium spacing of the atoms in the crystal lattice, which is of the order of a lattice constant, the nuclear repulsion is small because the positive nuclear charges are nearly completely shielded by the intervening electrons [Fig. 17.4(c)]. In this region the potential energy of interaction is adequately represented by the Born–Mayer potential:

$$V(r) = A \exp\left(-\frac{r}{\rho}\right) \qquad (17.32)$$

Although the constants A and ρ in this formula cannot be determined from theory, they can be obtained from the equilibrium properties of the solid (Chap. 4).

As the separation distance between the two atoms decreases, the closed-shell repulsion described by Eq. 17.32 increases but, since there are fewer electrons between the two nuclei to shield the positive charges from each other, so does the electrostatic repulsion contribution to the potential energy. When the interaction energy is so large that the two nuclei are separated by distances smaller than the radius of the inner electron shells (the K-shells), the principal contribution to the total potential energy of the system is due to the electrostatic force between the two positively charged nuclei [Fig. 17.4(a)]. In this limit the interaction is satisfactorily described by the Coulomb potential:

$$V(r) = \frac{Z_1 Z_2 e^2}{r} \qquad (17.33)$$

where Z_1 and Z_2 are the atomic numbers of the two atoms or ions and e is the electronic charge ($e^2 = 14.4$ eV-Å).

The intermediate region where both Coulombic repulsion and closed-shell repulsion are of comparable magnitudes is the most difficult to describe accurately. Unfortunately, these separation distances are just those most likely to occur in radiation-damage situations. This region, which is depicted in Fig. 17.4(b), is often represented by the screened Coulomb potential, which reflects the diminution of the pure Coulomb repulsion between the nuclei due to the electrostatic screening of the positive charges by the intervening inner-shell electrons. This potential is given by

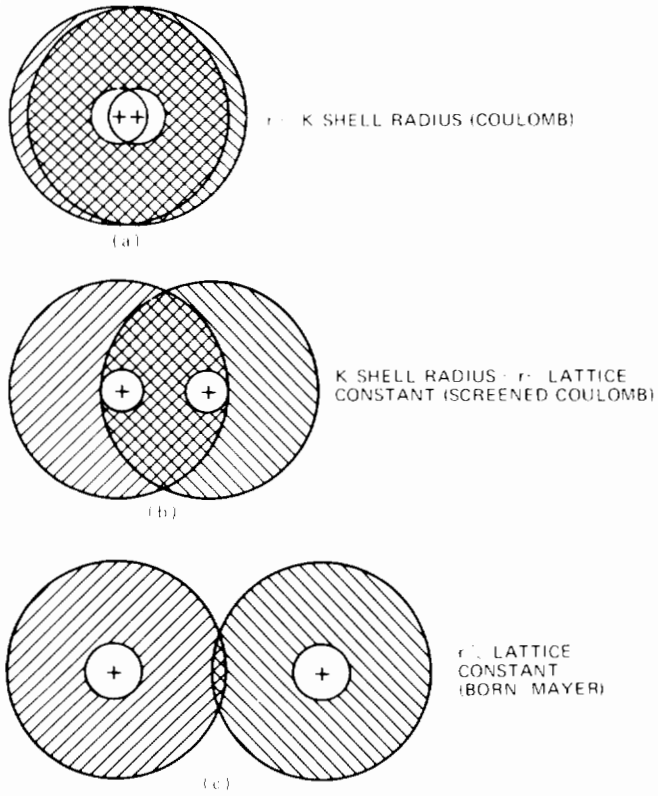

Fig. 17.4 Regions of applicability of various interatomic potential functions. The + sign represents the nuclear charge, and the shaded annular zones depict the radii between the innermost electronic shells and the ionic radius, where most of the atomic electrons are located. The cross-hatched areas dencte the regions of overlap of the electron clouds of the two atoms.

$$V(r) = \frac{Z_1 Z_2 e^2}{r} \exp\left(-\frac{r}{a}\right) \qquad (17.34)$$

where a is the screening radius, given by

$$a = \frac{2^{1/2} \lambda a_B}{(Z_1^{2/3} + Z_2^{2/3})^{1/2}} \qquad (17.35)$$

where a_B is the Bohr radius and λ is a constant of order unity (values from 0.707 to 2.09 have been used in various calculations). The screening radius decreases as the atomic numbers of the atomic species increase because the number of electrons with orbital radii less than a specified value r increases with the charge of the nucleus. As $r \ll a$, the screened Coulomb potential reduces smoothly to the Coulomb potential function.

Equation 17.34 does not account for the potential energy due to closed-shell repulsion, which decreases less rapidly than the potential arising from screened repulsion of the nuclear charges. Although Eq. 17.34 extends the range of the Coulomb potential somewhat, it falls off much more rapidly than the Born—Mayer potential. Hence, the screened Coulomb potential cannot be used to bridge the entire gap between the Coulomb and Born—Mayer potential functions. A number of theoretical and empirical potentials for describing this region have been proposed (Ref. 1, pp. 95-105; Ref. 2, Chap. 6, and Refs. 8 and 9).

Inverse power potentials of the form

$$V(r) = \frac{A}{r^s} \qquad (s = 2,3) \qquad (17.36)$$

have also beeen used extensively. The constants A and s are obtained by fitting Eq. 17.36 to the screened Coulomb potential at small r or to the Born—Mayer potential function at large r. In this manner the entire interatomic potential can be spliced together by a series of functions of different form (Fig. 17.5).

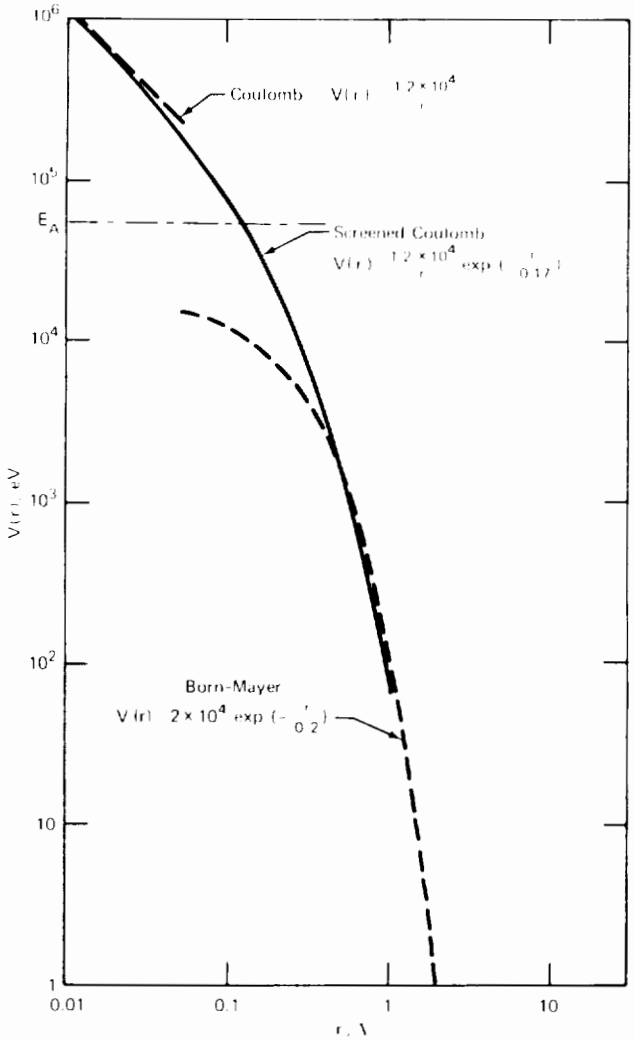

Fig. 17.5 Composite potential function for interaction between copper atoms.

17.4.2 Energy-Transfer Cross Sections

It is in principle possible to transform any of the potentials described in the preceding section into a differential angular cross section $\sigma(E,\theta)$ and then to a differential energy-transfer cross section (see Ref. 1, pp. 105-107). However, only the Coulomb and inverse power potentials yield analytical formulas for $\sigma(E,T)$. The Coulomb poten-

tial leads to the familiar Rutherford scattering cross section:

$$\sigma(E,T) = \pi Z_1^2 Z_2^2 e^4 \left(\frac{M_1}{M_2}\right) \frac{1}{ET^2} \qquad (17.37)$$

The inverse power potential of Eq. 17.36 yields the differential cross section:

$$\sigma(E,T) = \text{Constant} \frac{1}{E^{1/s}} \frac{1}{T^{1+(1/s)}} \qquad (17.38)$$

A form of the differential energy-transfer cross section which is particularly convenient for radiation-damage problems is based on the billiard-ball dynamics of hard spheres. This potential is $V = \infty$ for $r < 2r_o$ and $V = 0$ for $r > 2r_o$, where r_o is the radius of the colliding hard spheres. It is well known that the angular cross section for hard-sphere scattering is isotropic in the center-of-mass system, or $\sigma(E,\theta) = \pi(2r_o)^2/4\pi$. Introducing this expression into Eq. 17.22 yields the energy-transfer cross section:

$$\sigma(E,T) = \frac{4\pi r_o^2}{\Lambda E} = \frac{\sigma(E)}{\Lambda E} \qquad (17.39)$$

The major computational advantage of Eq. 17.39 is its lack of dependence on T, which considerably simplifies the integrals required to determine energy loss and collisional properties of radiation damage. The prime disadvantage of this formula, of course, is that it is based on an unrealistic interatomic potential function.

The utility of the hard-sphere model can be retained and yet some flavor of the correct interatomic potential can be introduced by allowing the hard-sphere radius r_o to vary with particle energy. This so-called equivalent or energy-dependent hard-sphere model can be applied to any interatomic potential function. The recipe for determining r_o is to equate $2r_o$ to the distance of closest approach in a head-on collision. The latter is determined from the actual potential function $V(r)$. For identical atoms, $V(2r_o) = E/2$ (Eq. 17.17), which serves to fix r_o as a function of E. For the screened Coulomb potential, this procedure yields

$$\frac{Z^2 e^2}{E} = r_o(E) \exp\left[\frac{2r_o(E)}{a}\right] \qquad (17.40)$$

where $Z_1 = Z_2$ for collisions between like atoms.

For the Born—Mayer potential of Eq. 17.32, the equivalent hard-sphere radius is

$$r_o(E) = \frac{1}{2}\rho \ln\left(\frac{2A}{E}\right) \qquad (17.41)$$

The energy-transfer cross section is given when Eq. 17.39 is combined with either Eq. 17.40 or 17.41.

Collisions become more hard-sphere-like as the potential function steepens. Figure 17.5 shows that $V(r)$ is changing most rapidly with r at low energies, where the inverse power or Born—Mayer potentials are applicable. The Coulomb potential, which varies as r^{-1}, cannot be adequately approximated by an equivalent hard sphere. The crudest approacb to delineating the energy below which the equivalent hard-sphere model can be employed is to equate the screening radius with the distance of closest approach in a head-on collision in pure screened Coulomb scattering. The latter can be obtained from Eqs. 17.17 and 17.34 as a solution of

$$\frac{Z^2 e^2 \exp(-x_m/a)}{x_m} = \frac{E}{2}$$

Setting $x_m = a$ and determining a from Eq. 17.35 for $Z_1 = Z_2$ and $\lambda = 1$ yields the critical energy separating Rutherford and hard-sphere scattering when projectile and target atoms are the same kind:

$$E_A = \frac{2Z^{7/3} e^2 \exp(-1)}{a_B} \qquad (17.42)$$

Figure 17.5 shows the transition for copper at ~50 keV. Although the hard-sphere model is to be used for projectile energies less than the value given by Eq. 17.42, the total cross section can vary with energy according to r_o formulas, such as Eqs. 17.40 and 17.41, or the equivalent expression for an inverse power potential.

The principal difference between the energy-transfer cross sections derived from realistic potentials, such as the Coulomb and inverse power functions, and from the hard-sphere model is the dependence upon T. Equation 17.39 shows that all energy transfers between 0 and $T_m = \Lambda E$ are equally probable, whereas Eqs. 17.37 and 17.38 strongly favor forward scattering, in which the energy transfer is small. Despite the shortcomings of the hard-sphere model, the fact that it considerably simplifies the analysis makes it valuable for qualitatively demonstrating the salient features of radiation-damage processes.

17.5 ENERGY LOSS TO ELECTRONS

The rate at which high-velocity heavy particles lose energy to the electrons of the medium through which they are travelling is important in many radiation-damage calculations; the range of a charged particle in matter is primarily determined by $(dE/dx)_e$ (Eq. 17.30). The ability of a primary knock-on atom to create displacements in the lattice is in part determined by the fraction of the initial energy of the PKA which is dissipated in electronic interactions during slowing down.

The complexity of accurately accounting for electronic energy losses in cascade theory can be avoided by the simple expedient of determining an energy E_c below which the moving atom cannot transfer enough energy to an electron of the medium to remove the latter from whatever bound state it may be in. Let I be the binding energy of an electron to an atom of the solid. For an electron to acquire energy I in a head-on collision with a moving atom of mass M_1, the energy of the atom must be (Eqs. 17.8 and 17.10 with $E = E_c$ and $M_2 = m_e$, the electron mass):

$$E_c = \frac{M_1}{4m_e} I$$

For ionic or covalent solids, the most reasonable choice for I is the energy needed to bridge the forbidden zone between the valence and conduction bands, which is several electron volts. In metals, electrons very near the top of the Fermi sea can be excited by any amount of energy, no

matter how small. However, the bulk of the conduction electrons in a metal lie well below the Fermi level, and excitation by arbitrarily small additions of kinetic energy is precluded by the fact that higher levels are occupied (Chap. 4). The average electron in metal, therefore, needs to receive about one-half the Fermi energy in order to become excited and thereby remove energy from the moving atom. Setting $m_e = 1/2000$ amu and $I = 2$ eV, we find the critical energy for all substances to be roughly equal to the mass number of the moving atom in kiloelectron volts:

$$E_c \simeq 10^3 M_1 \text{ (eV)} = M_1 \text{ (keV)} \qquad (17.43)$$

When the kinetic energy of the moving atoms or ions falls below this value, energy losses to the electrons of the solid rapidly become small compared to the energy that the moving atom can transfer to stationary atoms of the lattice by elastic collisions. As a corollary, energy transfer by atomic collisions for $E > E_c$ is presumed to be negligible compared to the electronic stopping of the moving particle.

It will be shown later that electronic energy loss in metals continues for energies below the value given by Eq. 17.43 and that this loss mode is important in assessing the amount of damage that can be inflicted by nuclear radiations. It is therefore useful to analyze energy transfer to the electrons of a solid on a more realistic basis than that described above. Two calculations of $(dE/dx)_e$ are reviewed below.

17.5.1 Electronic Stopping at High Energies

When a heavy particle at high energy (i.e., more than several million electron volts) penetrates a solid, the great velocity strips off its outer orbital electrons. As a consequence, it moves through the solid as an ion whose charge is denoted as Z_1 (this is not the atomic number of the moving atom). The moving ion transfers energy to the electrons of the medium by Coulombic interaction. The energy-transfer cross section for the process is given by Eq. 17.37 in which the second particle is an electron ($Z_2 = 1$, $M_2 = m_e$). Thus,

$$\sigma(E,T_e) = \frac{\pi Z_1^2 e^4 (M_1/m_e)}{ET_e^2} \qquad (17.44)$$

where E is the energy of the moving ion and T_e is the energy transferred to the electron during the binary encounter. If the ion energy is sufficiently high, all the electrons in the solid can be excited, and the density of electrons is ZN, where N is the atom density of the solid and Z is the atomic number of the atoms of the solid. The electronic stopping power is given by Eq. 17.29 in which $T_m = 4(m_e/M_1)E$ and $T_0 = \bar{I}$, the average ionization energy of the target atoms. The energy-transfer cross section is given by Eq. 17.44 so the electronic stopping power can be expressed by

$$\left(\frac{dE}{dx}\right)_e = ZN \int_{\bar{I}}^{4(m_e/M_1)E} T_e \left[\frac{\pi Z_1^2 e^4 (M_1/m_e)}{ET_e^2}\right] dT_e$$

Performing the integration yields

$$\left(\frac{dE}{dx}\right)_e = \frac{\pi N Z_1^2 Z e^4 (M_1/m_e)}{E} \ln\left[\frac{4E}{(M_1/m_e)\bar{I}}\right] \qquad (17.45)$$

When multiplied by a factor of 2 (which arises when the correct quantum-mechanical calculation is performed instead of the above classical analysis), Eq. 17.45 is known as Bethe's formula.

As the ion loses energy, the probability of capturing an electron from the medium increases. Or, the charge Z_1 is dependent on the energy of the ion. Bohr[10] has calculated an effective charge (so called because it need not be an integer) by assuming that the ion retains in its outer shell only those electrons with orbital velocities that exceed the velocity of the moving ion. The Thomas–Fermi distribution of the velocities of electrons in atoms permits the number of electrons in the atom with velocities less than the ion velocity $(2E/M_1)^{1/2}$ to be computed. These electrons are assumed to be stripped from the ion. The effective charge of the moving ion is given by

$$(Z_1)_{eff} = \frac{Z_1^{1/3}\hbar}{e^2}\left(\frac{2E}{M_1}\right)^{1/2} \qquad (17.46)$$

where $\hbar$ is Planck's constant divided by 2π and Z_1 now denotes the atomic number of the moving ion. Electron capture and loss from an atom or ion moving in a solid are dynamic processes, and noninteger charges should be interpreted as a result of weighting integer charge states (including the neutral atom) with the fraction of the time that is spent in each charge state. The effective charge cannot exceed the atomic number of the moving ion, of course, but Eq. 17.46 indicates that the ion will retain some charge no matter how low its kinetic energy. Actually, there is a lower energy, E_{neut}, at which a neutralized moving atom cannot be reionized by impact with a stationary electron in the solid. Consider the collision of the most weakly bound electron in the moving atom with a stationary electron in the medium. Instead of the atom traversing a sea of stationary electrons with a velocity $v_1 = (2E/M_1)^{1/2}$, consider the atom to be stationary and let the lattice electrons move with velocity v_1 (i.e., change the frame of reference from the laboratory to the moving atom). If one of the lattice electrons makes a head-on collision with an electron in the atom, energy equal to $m_e v_1^2/2$ is transferred from the former to the latter. If this quantity of energy is less than the minimum ionization energy of the moving atom, I, reionization cannot occur and the atom remains neutral for the remainder of the slowing-down process. The condition

$$\frac{1}{2} m_e v_1^2 = E_{neut} \frac{m_e}{M_1} = I$$

leads to numerical values of E_{neut} very similar to those determined for the opposite process (ionization of a lattice atom by a moving atom). Within the framework of this simple treatment, the minimum energy that a moving particle needs in order to maintain some positive charge is approximately given by its mass number in kiloelectron volts:

$$E_{neut} = M_1 \text{ (keV)} \qquad (17.47)$$

Below this energy, $(Z_1)_{eff}$ is zero and Eq. 17.46 does not apply.

Actually, Eq. 17.45 ceases to be valid at much greater energies than the tens of kiloelectron volts suggested by simple consideration of charge neutralization. The Bethe formula is in fact valid only on the portion of the stopping power curve where $(dE/dx)_e$ is decreasing with energy. For heavy ions this occurs at energies[8] as high as 100 meV. The PKA created by fast neutrons scattering from the atoms of a metal are generally not energetic enough to fall in the range of applicability of Eq. 17.45; so a different mechanism is needed to explain the electronic stopping of predominantly neutral atoms passing through a lattice consisting of the same species.

17.5.2 Electronic Stopping at Low Energies

In order to compute $(dE/dx)_e$ for atoms or ions moving in a metal of the same type, we compute the energy transfer to the conduction electrons very near the Fermi surface. As noted previously, these electrons can become excited by collisions that transfer considerably less energy than the energy needed to excite the average conduction electron (which requires $\sim\epsilon_F/2$). Consider an atom of mass M_1 and velocity v_{10} which makes a head-on collision with a conduction electron moving in the opposite direction with a velocity v_e. According to Eq. 17.12, with $v_1 = v_{10}$ and $v_2 = -v_e$, the initial relative speed of the two particles is $g_0 = v_{10} + v_e$. In a head-on collision, the relative velocity vector changes sign but not magnitude; thus $g_f = -(v_{10} + v_e)$. The speed of the atom following the collision with the electron is given by Eq. 17.13a:

$$\begin{aligned} v_{1f} &= v_{cm} + \left(\frac{m_e}{M_1 + m_e}\right) g_f \\ &= \frac{M_1 v_{10} - m_e v_e}{M_1 + m_e} - \left(\frac{m_e}{M_1 + m_e}\right)(v_{10} + v_e) \\ &= v_{10} - \frac{2m_e v_e}{M_1} \end{aligned}$$

where m_e has been neglected compared to M_1. The energy loss suffered by the atom in the collision is

$$\begin{aligned} \Delta E = \Delta\left(\frac{1}{2} M_1 v_1^2\right) &\sim M_1 v_{10}(v_{10} - v_{1f}) \\ &= 2m_e v_e v_{10} \end{aligned} \qquad (17.48)$$

Similarly, the electron velocity after the collision is given by Eq. 17.13b:

$$\begin{aligned} v_{ef} &= v_{cm} - \left(\frac{M_1}{M_1 + m_e}\right) g_f \\ &= \frac{M_1 v_{10} - m_e v_e}{M_1 + m_e} + \left(\frac{M_1}{M_1 + m_e}\right)(v_{10} + v_e) \\ &= 2v_{10} + v_e \end{aligned}$$

Or, the increase in the velocity of the electron is

$$\Delta v_e = v_{ef} - v_e = 2v_{10} \qquad (17.49)$$

In a monovalent metal the number of conduction electrons is approximately equal to the atom density N. However, only those electrons with velocities lying in the range Δv_e of the Fermi velocity v_F are able to participate in the slowing-down process. Or, the density of effective electrons in the metal is

$$n_e \sim N\left(\frac{\Delta v_e/2}{v_F}\right) = \left(\frac{v_{10}}{v_F}\right) N \qquad (17.50)$$

Now consider a reference frame attached to the moving atom. The current of effective electrons impinging on the atom is

$$I_e = n_e g_0 = n_e(v_{10} + v_e) \sim n_e v_e \qquad (17.51)$$

and the number of collisions of the effective electrons per second with a single moving atom is $\sigma_e I_e$, where σ_e is the cross section for the interaction of the moving atom with the conduction electrons. The rate at which a moving atom loses energy to the effective electrons is $\sigma_e I_e\ \Delta E$, which, when divided by the distance moved by the atom in 1 sec (v_{10}), gives the stopping power:

$$\left(\frac{dE}{dx}\right)_e = \frac{\text{Energy loss/sec-atom}}{\text{Distance travelled/sec-atom}} = \frac{\sigma_e I_e\ \Delta E}{v_{10}}$$

Substituting Eqs. 17.48, 17.50, and 17.51 into the above formula and expressing v_e and v_{10} as $2\epsilon_F/m_e$ and $(2E/M_1)^{1/2}$, respectively, yields

$$\left(\frac{dE}{dx}\right)_e = 8\sigma_e N\left(\frac{m_e}{M_1}\right)^{1/2} E^{1/2}$$

Or, writing the coefficient of $E^{1/2}$ as a constant k, the stopping power becomes

$$\left(\frac{dE}{dx}\right)_e = k\,E^{1/2} \qquad (17.52)$$

More accurate analyses of this stopping mechanism than the simple model described above produce different values for the constant k, but the dependence upon $E^{1/2}$ remains (see Ref. 9 for a review of this subject). For like atoms the k-value derived by Lindhard is

$$k = 0.3NZ^{2/3},\ eV^{1/2}/\text{Å} \qquad (17.53a)$$

where N is the atomic density of the metal in units of Å^{-3} and Z is the atomic number of the atoms of the metal. Equations 17.52 and 17.53 are valid for the energy range

$$0 < E(\text{keV}) < 37Z^{7/3} \qquad (17.53b)$$

In this formula and in Eq. 17.53a, use has been made of the fact that $Z/M = 0.43 \pm 0.03$ for all elements except hydrogen.

17.6 THE DISPLACEMENT THRESHOLD

All analytical cascade theories are based on the assumption that a lattice atom struck by a PKA or a higher order recoil must receive a minimum amount of energy in the collision in order to be displaced from its lattice site. This quantity of energy is called the displacement energy or the displacement threshold and is denoted by E_d. If the energy transfer, T, is less than E_d, the struck atom undergoes large amplitude vibrations without leaving the potential well forming its stable lattice position. The vibrational energy is

quickly communicated to the nearest neighbors of the struck atom and appears as a localized source of heat. On the other hand, if $T > E_d$, the struck atom is able to pass over the potential barrier and move off into the lattice as a displaced atom.

Because of the crystallographic structure of the solid, the potential barrier surrounding a lattice atom in its equilibrium position is not uniform in all directions. If the struck atom moves off in a direction where its nearest neighbors are favorably disposed to remove energy from the struck atom before it escapes, the barrier is high. However, the potential barrier in a direction of high lattice symmetry resembles a mountain pass. These "saddle points" where the displacement threshold is low may be along either relatively open direction, such as the ⟨111⟩ directions in the fcc lattice, or along close-packed directions, such as the ⟨110⟩ directions in the same structure. The direction acquired by the recoil is dictated by the dynamics of the collision and hence is random in the sphere surrounding the equilibrium site. The single value of the displacement energy used in radiation-damage theory is in reality a spherical average of the saddle points in the potential barrier surrounding the equilibrium lattice site.

The displacement energy can in principle be computed if the interaction potential between atoms of the lattice is known. The procedure is to move the atom from its equilibrium position in a chosen direction and sum the interaction energies between the moving atoms and all the nearest neighbors for each position along the line (or curve) representing the trajectory of the struck atom. When the total potential energy reaches a maximum, the position corresponds to a saddle point, and the difference between the energy of the atom at the saddle point, ϵ^*, and its energy in the equilibrium position, ϵ_{eq}, represents the displacement threshold for the particular direction. Such calculations are usually carried out by computer[11,12] using a Born–Mayer potential to represent the repulsive forces between the struck atom and the nearest neighbors it encounters during motion. Because the interaction energies involved in these threshold calculations are only tens of electron volts, the Born–Mayer potential is the correct one to use.

In this section we illustrate the basic features of such calculations by using a simpler (but unrealistic) description of the interaction between neighboring atoms.

The atom in the lower left-hand corner of Fig. 17.6(a) is assumed to receive energy by collision with an energetic recoil and to start to move in a direction in the octant of the sphere represented by the unit cell in the drawing. We calculate the potential energy of the struck atom, which is moving in the [111] direction. The saddle point for this direction is the center of the triangle formed by the three nearest neighbors to the struck atom, which are connected by the wavey lines in Fig. 17.6(a). The energy of the struck atom as a function of position along the [111] direction is shown schematically in Fig. 17.6(b).

To describe the interaction energies, we describe the solid by the simple bond theory used primarily for covalent substances. In this theory, cohesion of the solid is the result of bonds of strength D acting in pairs between nearest neighbors. In an fcc lattice, each atom is surrounded by 12 nearest neighbors; thus the energy of a single atom in a normal lattice site is

$$\epsilon_{eq} = -12D \tag{17.54}$$

The zero in energy is taken as the isolated atom. In the bond theory of solids, the bond energy may be computed from the energy of sublimation (Eq. 4.45 and Table 4.1).

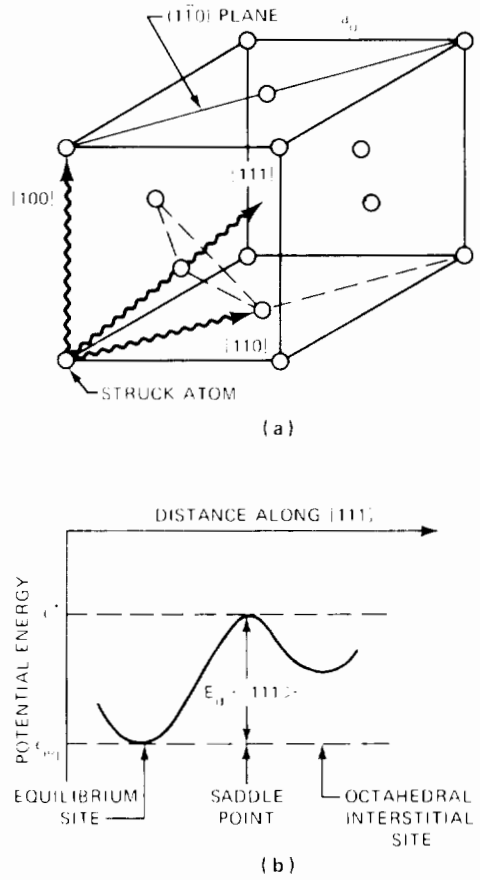

Fig. 17.6 Displacement of a lattice atom recoiling from a collision with an energetic atom.

This quantity is just half the energy of an interior atom since sublimation represents removal of an atom from the surface, a process that involves breaking only half as many bonds as is necessary in removing an atom from the inside of the solid. Thus, for the fcc lattice

$$\Delta E^{\circ}_{sub}\,(0^{\circ}K) = 6D \tag{17.55}$$

Since the sublimation energy of metals in the transition region of the periodic table is 5 to 6 eV, the bond energy in the fcc lattice is $D \simeq 1$ eV. When atoms of the lattice are pushed closer to each other than the equilibrium nearest-neighbor distance, r_{eq}, the potential energy increases. Instead of using a Born–Mayer potential to describe this repulsion, we use a simple parabolic repulsion. The interaction potential between two lattice atoms is represented by

$$V(r) = -D + \frac{1}{2}k(r_{eq} - r)^2 \qquad (\text{for } r < r_{eq})$$
$$V(r) = 0 \qquad (\text{for } r > r_{eq}) \tag{17.56}$$

where the force constant k characterizing the repulsive portion of the potential can be computed as follows. Atoms in the crystal can be made to approach each other more closely than r_{eq} either by the movement of an energetic atom in the crystal (which is pertinent to the displacement threshold computation) or in a uniform manner by exerting external pressure to compress the entire crystal. The resistance of the solid to compression is measured by the compressibility, β. In Chap. 4 we showed that compressibility is related to the second derivative of the crystal energy by

$$\frac{1}{\beta} = v_{eq}\left(\frac{d^2U}{dv^2}\right)_{eq}$$

where U is the energy per atom of the crystal when the specific volume is v. For the fcc lattice, $v = a_o^3/4$, where a_o is the lattice constant. The nearest-neighbor separation distance is $r = a_o/2^{1/2}$; thus $v = r^3/2^{1/2}$. The above formula can therefore be written in terms of r as

$$\frac{1}{\beta} = \frac{2^{1/2}}{9}\frac{1}{r_{eq}}\left(\frac{d^2U}{dr^2}\right)_{eq}$$

In the bond model of the fcc solid, the crystal energy U(r) is equal to $12V(r)/2 = 6V(r)$, and the compressibility is given by

$$\frac{1}{\beta} = \frac{6(2)^{1/2}}{9r_{eq}}\left(\frac{d^2V}{dr^2}\right)_{eq} = \frac{2(2)^{1/2}k}{3r_{eq}} = \frac{4k}{3a_o} = \frac{ka_o^2}{3v_{eq}}$$

Thus the force constant of the repulsive portion of the interaction potential is

$$ka_o^2 = \frac{3v_{eq}}{\beta}$$

Typical values of v_{eq} and β for metals are ~ 15 Å^3 and $\sim 5 \times 10^{-13}$ cm^2/dyne, respectively, which yield $ka_o^2 \sim 60$ eV. We assume that the potential function of Eq. 17.56, in which the constants were obtained from the equilibrium properties of heat of sublimation and compressibility, is applicable to the interaction of the moving atom in the lattice.

When the atom is at the center of the triangle shown in Fig. 17.6(a), it interacts with the three atoms at the corners a distance $a_o/6^{1/2}$ away. The energy at the saddle point is

$$\epsilon^* = 3V\left(\frac{a_o}{6^{1/2}}\right) = 3\left[-D + \frac{1}{2}(ka_o^2)\left(\frac{1}{2^{1/2}} - \frac{1}{6^{1/2}}\right)^2\right]$$

The displacement energy in the [111] direction is thus

$$E_d\langle 111\rangle = \epsilon^* - \epsilon_{eq} = 9D + \frac{3}{2}(ka_o^2)\left(\frac{1}{2^{1/2}} - \frac{1}{6^{1/2}}\right)^2$$

Using the values of D and ka_o^2 computed above, this equation gives $E_d\langle 111\rangle = 15.6$ eV. Displacement thresholds calculated by computer for copper are shown in Table 17.1. The figures shown in the last two columns of the table indicate that displacement is considerably easier when the direction of the struck atom is along a line of atoms in the crystal (i.e., the ⟨100⟩ and ⟨110⟩ directions) than it is in the open ⟨111⟩ directions. The ease of displacement in the former directions is explained by the phenomenon of focusing whereby replacement of the next atom in the line by the struck atom is followed by replacement of the third atom by the second, etc.

Displacement thresholds corresponding to initial directions other than the three illustrated in Fig. 17.6(a) and Table 17.1 can be obtained by similar computational techniques. A schematic representation of the results for all directions in the plane formed by the [100], [111], and [1$\bar{1}$0] directions in Fig. 17.6(a) [i.e., directions lying in the (1$\bar{1}$0) plane] is shown in Fig. 17.7. Local minimums in the displacement energies are found in the [110], [111], and [$\bar{1}$10] directions. Similar calculations out of the (1$\bar{1}$0) plane show that the minimums along these crystallographic directions are true troughs, not saddle points. The single threshold energy used in most radiation-damage calculations represents the average of results such as those shown in Fig. 17.7 and comparable out-of-plane profiles over all polar and azimuthal angles in the octant delineated by the unit cell with the struck atom at one corner.

The directional dependence of E_d, coupled with the randomness of the initial directions of the struck atom, implies that the notion of a sharp displacement threshold is

Table 17.1 Displacement Threshold Energies in Copper

Direction	Displacement energy, eV		
	Ref. 11*	Ref. 12	Ref. 13†
$E_d\langle 100\rangle$	18, 34	24	15, 34
$E_d\langle 111\rangle$	19, 43	80	70, 52
$E_d\langle 110\rangle$		25	31, 15

*The two values were obtained by two sets of the constants A and ρ in the Born–Mayer potential function of Eq. 17.32.

†These constants were determined by fitting radiation-damage data. The two sets of threshold energies listed fit the data equally well.

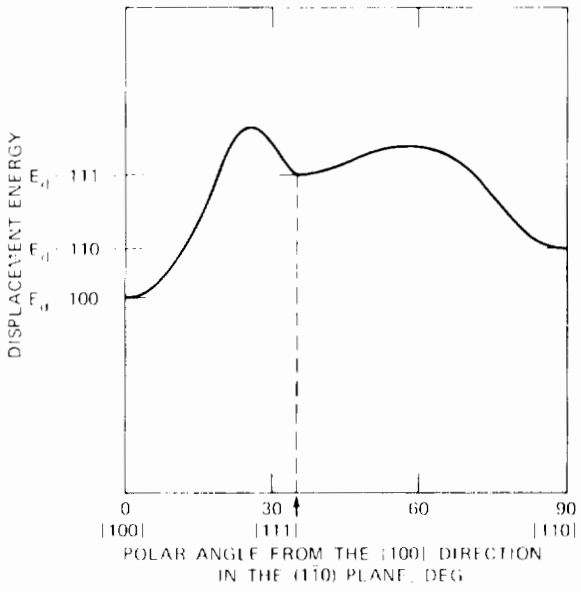

Fig. 17.7 Directional dependence of the displacement threshold.

oversimplified. Rather, there is a range of displacement energies, from $E_{d(min)}$ to $E_{d(max)}$, for which displacement may occur. For example, in Fig. 17.7, $E_{d(min)}$ corresponds to $E_d\langle 100\rangle$ and $E_{d(max)}$ to an $\sim 30^\circ$ polar angle. This smearing out of the displacement threshold due to crystallographic direction of the struck atom is commonly incorporated into radiation-damage calculations by defining a displacement probability, $P_d(T)$, which gives the probability that a struck atom is displaced upon receipt of energy T. This probability $P_d(T)$ is taken to be of the form

$$\begin{aligned} P_d(T) &= 0 \quad [\text{for } T < E_{d(min)}] \\ &= f(T) \quad [\text{for } E_{d(min)} < T < E_{d(max)}] \\ &= 1 \quad [\text{for } T > E_{d(max)}] \end{aligned} \tag{17.57}$$

Sosin[14] lists seven different functions f(T) which have been used to generate displacement probability curves. The single displacement energy concept most commonly used in damage analyses corresponds to a step-function displacement probability in which $E_{d(min)} = E_{d(max)} = E_d$:

$$\begin{aligned} P_d(T) &= 0 \quad (\text{for } T < E_d) \\ &= 1 \quad (\text{for } T > E_d) \end{aligned} \tag{17.58}$$

In this model, E_d is fixed at a value between 25 and 50 eV, the lower figure being the one most commonly used.

17.7 DISPLACEMENTS PRODUCED BY A PRIMARY KNOCK-ON

The crux of the damage-producing effect of fast neutrons and fission fragments is the production of displaced atoms by the primary knock-ons. In this section the theoretical basis for calculating the total number of displaced atoms resulting from a single PKA of energy E is reviewed. The number of displaced atoms is denoted by $\nu(E)$.

17.7.1 Elementary Theory

The simplest theory of the displacement cascade is that due to Kinchin and Pease.[15] Their analysis is based on the following assumptions:

1. The cascade is created by a sequence of two-body elastic collisions between atoms.

2. The displacement probability is given by Eq. 17.58.

3. The energy E_d consumed in displacing an atom is neglected in the energy balance of the binary collision that transfers kinetic energy to the struck atom.

4. Energy loss by electron stopping is treated by the cutoff energy of Eq. 17.43. If the PKA energy is greater than E_c, no displacements occur until electronic energy losses reduce the PKA energy to E_c. For all energies less than E_c, electronic stopping is ignored, and only atomic collisions take place.

5. The energy-transfer cross section is given by the hard-sphere model.

6. The arrangement of the atoms in the solid is random; effects due to the crystal structure are neglected.

Later on in this section, we will relax restrictions (3), (4), and (5). In the subsequent section, assumption (6) will be removed from the analysis. Assumption (1) is fundamental to all theories of a cascade consisting of isolated point defects. When this restriction is eliminated, the cascade resembles a displacement spike, which is treated at the end of this chapter.

The cascade is initiated by a single PKA of energy E, which eventually produces $\nu(E)$ displaced atoms. At some time during the development of the cascade, the number of energetic, moving atoms is larger than 1 but less than $\nu(E)$, and the average kinetic energy of the moving atoms is less than E but still not zero. However, the population of moving atoms at any intermediate stage will ultimately produce the same number of stationary displaced atoms as the original PKA, namely, $\nu(E)$. Therefore, the quantity $\nu(E)$ is conserved in the sense that it can be determined by starting with the energy distribution of the moving atoms at any time after birth of the PKA but before the final displaced configuration is achieved. In particular, $\nu(E)$ can be determined by considering the two moving atoms that are created when the PKA first strikes a stationary lattice atom (Fig. 17.8). Thus, if the PKA of energy E transfers energy T to the struck atom and leaves the collision with energy $E - T$, we can say that

$$\nu(E) = \nu(E - T) + \nu(T) \tag{17.59}$$

Note that the energy E_d required to displace the struck atom has not been deducted from the energy of the recoil [assumption (3)]. Had this energy loss been included, the last term in Eq. 17.59 would be written as $\nu(T - E_d)$.

Equation 17.59 does not suffice to determine $\nu(E)$ because the energy transfer T is not specified. Since the PKA and the lattice atoms are identical, T can be anywhere from 0 to E. However, if we know the probability of transferring energy between T and T + dT in a collision, we can multiply Eq. 17.59 by this probability and integrate over all permissible values of T. Invoking the hard-sphere assumption (5), the energy-transfer cross section is given by Eq. 17.39, and the probability that a PKA of energy E transfers energy in the range (T,dT) to the struck atom is

$$\frac{\sigma(E,T)\,dT}{\sigma(E)} = \frac{dT}{E} \quad (\text{for } A = 1) \tag{17.60}$$

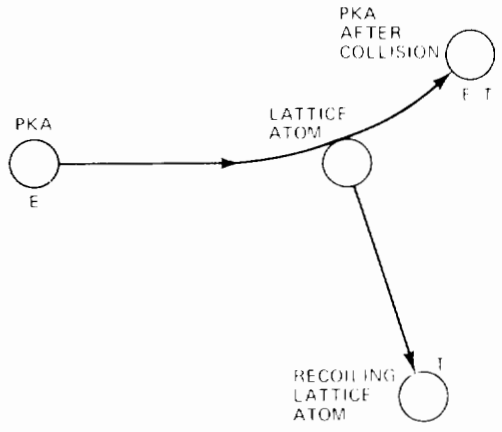

Fig. 17.8 Before and after the first collision of a cascade.

Multiplying the right-hand side of Eq. 17.59 by dT/E and integrating from 0 to E yields

$$\nu(E) = \frac{1}{E}\int_0^E [\nu(E-T) + \nu(T)]\,dT \qquad (17.61)$$

The right side of this equation consists of two integrals, which may be shown to be identical by changing the variable of integration in the first from T to $T' = E - T$, and Eq. 17.61 reduces to

$$\nu(E) = \frac{2}{E}\int_0^E \nu(T)\,dT \qquad (17.62)$$

Before attempting to solve this integral equation, we first consider the behavior of $\nu(E)$ near the threshold energy E_d. Clearly when $E < E_d$, not even the PKA is displaced, and

$$\nu(E) = 0 \qquad (\text{for } 0 < E < E_d) \qquad (17.63)$$

When the PKA is born with an energy between E_d and $2E_d$, the first collision with a lattice atom has one of two possible results: If energy in excess of E_d, but necessarily less than $2E_d$, is transferred to the lattice atom, the latter is displaced, but the initial PKA is left with energy less than E_d. The struck atom moves off its lattice site, but the PKA falls into the vacated site, dissipating its remaining kinetic energy as heat. Conversely, if the original PKA transfers less than E_d, the struck atom is not displaced. In either of the above two possibilities, the first PKA collision results in only one moving atom, which has an energy less than the original PKA. The same arguments advanced above can be applied to the second-generation moving atom, and the conclusion is that it too is incapable of creating any additional displacements. Therefore, a PKA with kinetic energy between E_d and $2E_d$ produces only one displaced atom, or

$$\nu(E) = 1 \qquad (\text{for } E_d < E < 2E_d) \qquad (17.64)$$

We may split the integral in Eq. 17.62 into ranges from 0 to E_d, E_d to $2E_d$, and $2E_d$ to E and evaluate the first two using Eqs. 17.63 and 17.64. Thus we arrive at

$$\nu(E) = \frac{2E_d}{E} + \frac{2}{E}\int_{2E_d}^E \nu(T)\,dT \qquad (17.65)$$

This equation can be solved by multiplying by E and differentiating with respect to E, which yields the differential equation

$$E\frac{d\nu}{dE} = \nu \qquad (17.66)$$

the solution of which is

$$\nu = CE \qquad (17.67)$$

The constant C is obtained by substitution of Eq. 17.67 into Eq. 17.65, which shows $C = (2E_d)^{-1}$. Therefore the number of displacements is

$$\nu(E) = \frac{E}{2E_d} \qquad (\text{for } 2E_d < E < E_c) \qquad (17.68)$$

The upper limit on the validity of Eq. 17.68 has been set equal to E_c since, by assumption (4), only electronic energy loss occurs for higher energies. When the PKA is born with an energy greater than E_c, the number of displacements is

$$\nu(E) = \frac{E_c}{2E_d} \qquad (\text{for } E > E_c) \qquad (17.69)$$

The Kinchin–Pease displacement function, which consists of Eqs. 17.63, 17.64, 17.68, and 17.69, is shown in Fig. 17.9. The scale is distorted to illustrate the four regions predicted by the model. If drawn to scale, the ionization cutoff E_c would be 10 to 20 times further out along the abcissa than shown in the drawing.

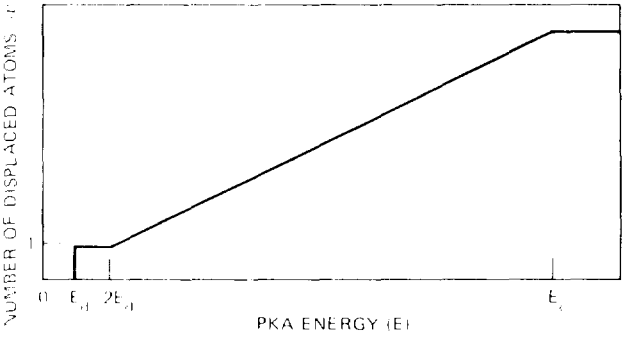

Fig. 17.9 The number of displaced atoms in the cascade as a function of PKA energy according to the model of Kinchin and Pease. (After Ref. 15.)

17.7.2 Use of a Realistic Energy-Transfer Cross Section

The hard-sphere assumption (5) can be removed by not introducing Eq. 17.60 into the analysis. In this case Eq. 17.61 should be written as

$$\nu(E) = \frac{1}{\sigma(E)}\int_0^E \sigma(E,T)\,[\nu(E-T) + \nu(T)]\,dT \qquad (17.70)$$

The arguments leading to Eqs. 17.63 and 17.64 are still valid (inasmuch as they depend only on energy conservation and not on the nature of the energy-transfer cross section), and the appropriate integral equation is

$$\nu(E) = \frac{2}{\sigma(E)}\int_{E_d}^{2E_d} \sigma(E,T)\,dT + \frac{1}{\sigma(E)}\int_{2E_d}^E \times \sigma(E,T)\,[\nu(E-T) + \nu(T)]\,dT \qquad (17.71)$$

This equation has been solved by Sanders[16] for the energy-transfer cross section based on the inverse power potential (Eq. 17.38). The result is

$$\nu(E) = s[2^{1/(1+s)} - 1]\left(\frac{E}{2E_d}\right) \qquad (\text{for } E_d < E < E_c) \qquad (17.72)$$

which, for $s = 2$, reduces the Kinchin–Pease result by a factor of ~2. Robinson[8] summarizes the extensive efforts that have been devoted to relieving cascade analysis of the hard-sphere assumption.

17.7.3 Energy Loss from the Cascade by Electronic Excitation

Relaxation of assumption (4) of cascade theory requires reformulation of the conservation principle for $\nu(E)$. In this case, collisions of the PKA with electrons compete

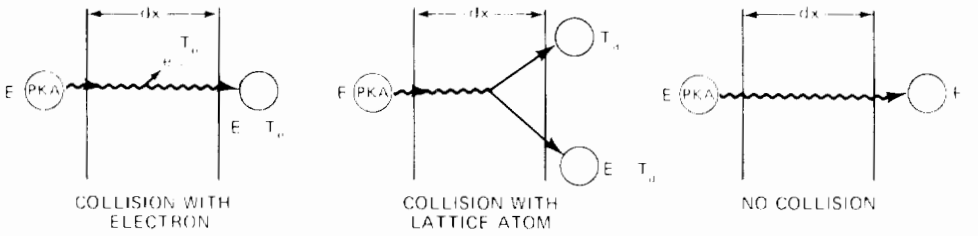

Fig. 17.10 Possible fates of a PKA on passing through a thickness dx of solid.

with atomic collisions with lattice atoms. As discussed in Sec. 17.1, these two processes can be treated independently, and each can be represented by separate energy-transfer cross sections. We formulate the basic integral equation in the manner originally presented by Lindhard et al.[17] by considering what happens to the PKA as it traverses a small distance dx of solid (Fig. 17.10). According to the basic definition of the differential energy-transfer cross section (Eq. 17.21), the probability $p_e\,dT_e$ that a collision between the PKA and an electron in the interval dx which transfers energy in the range (T_e, dT_e) to the electron is

$$p_e\,dT_e = N\,\sigma_e(E,T_e)\,dT_e\,dx \qquad (17.73)$$

where $\sigma_e(E,T_e)$ is the energy-transfer cross section from the PKA to an electron. Similarly, the probability of a collision in dx which transfers energy (T_a, dT_a) to a lattice atom is

$$p_a\,dT_a = N\,\sigma_a(E,T_a)\,dT_a\,dx \qquad (17.74)$$

In these equations, N is the density of atoms in the solid. The probability that nothing happens in dx is given by

$$p_0 = 1 - \int_0^{T_{em}} p_e\,dT_e - \int_0^{E} p_a\,dT_a$$

$$= 1 - N\,dx\left[\int_0^{T_{em}} \sigma_e(E,T_e)\,dT_e + \int_0^{E} \sigma_a(E,T_a)\,dT_a\right]$$

or

$$p_0 = 1 - N\,dx\,[\sigma_e(E) + \sigma_a(E)] \qquad (17.75)$$

where T_{em} is the maximum energy transferrable to an electron by a PKA of energy E and $\sigma_e(E)$ and $\sigma_a(E)$ are the total cross sections for collisions of the PKA with electrons and lattice atoms, respectively.*

We now apply the principle of conservation of $\nu(E)$ by requiring that this quantity be the same whether computed from the original PKA at its birth energy or whether it is determined by the products of the possible collisions that occur in dx. The ν-value associated with each of the recoil atoms in Fig. 17.10 is weighted with the appropriate probability for the process by which it is created and is integrated over the permissible ranges of the energy transfers. Thus

$$\nu(E) = \int_0^{E} [\nu(E - T_a) + \nu(T_a)]\,p_a\,dT_a + \int_0^{T_{em}} \nu(E - T_e)p_e\,dT_e + p_0\,\nu(E) \qquad (17.76)$$

*The analysis is not affected by the fact that the total cross section for energy transfer to electrons is infinite.

Substituting Eqs. 17.73 and 17.74 for p_e and p_a and Eq. 17.75 for p_0 yields

$$[\sigma_a(E) + \sigma_e(E)]\,\nu(E) = \int_0^{E} [\nu(E - T_a) + \nu(T_a)] \times \sigma_a(E,T_a)\,dT_a + \int_0^{T_{em}} \nu(E - T_e)\,\sigma_e(E,T_e)\,dT_e \qquad (17.77)$$

We now note that the maximum energy transferrable to an electron is very small compared to E; thus $\nu(E - T_e)$ can be expanded in a Taylor series and truncated after the second term:

$$\nu(E - T_e) = \nu(E) - \frac{d\nu}{dE}\,T_e \qquad (17.78)$$

The last term in Eq. 17.77 can therefore be written as

$$\int_0^{T_{em}} \nu(E - T_e)\,\sigma_e(E,T_e)\,dT_e = \nu(E)\int_0^{T_{em}} \sigma_e(E,T_e)\,dT_e - \frac{d\nu}{dE}\int_0^{T_{em}} T_e\,\sigma_e(E,T_e)\,dT_e \qquad (17.79)$$

The first integral on the right of Eq. 17.79 is the total cross section for collisions of the PKA with the electron. This term cancels the corresponding term on the left of Eq. 17.77. The second integral on the right of Eq. 17.79 is, according to Eq. 17.29, the electronic stopping power of the medium divided by the atom density, or $(dE/dx)_e/N$. When Eq. 17.79 is substituted into Eq. 17.77, the result is

$$\nu(E) + \left[\frac{(dE/dx)_e}{N\,\sigma(E)}\right]\frac{d\nu}{dE} = \int_0^{E} [\nu(E - T) + \nu(T)] \times \left[\frac{\sigma(E,T)}{\sigma(E)}\right] dT \qquad (17.80)$$

The subscript "a" on T and σ has been deleted with the understanding that these two quantities refer to atomic collisions. When $(dE/dx)_e$ is neglected, Eq. 17.80 reduces to Eq. 17.70, and, when, in addition, the hard-sphere model is used to fix the energy-transfer probability on the right side of the above equation, the original Kinchin—Pease formula, Eq. 17.61, is recovered.

To show the effect of electronic stopping on the number of displaced atoms, we solve Eq. 17.80 with the hard-sphere assumption retained but with $(dE/dx)_e$ given by the square-root law (Eq. 17.52). With this simplification, Eq. 17.80 reduces to

$$\nu(E) = \frac{2E_d}{E} + \frac{2}{E}\int_{2E_d}^{E} \nu(T)\, dT - \frac{k\, E^{1/2}}{\sigma N}\frac{d\nu}{dE} \qquad (17.81)$$

where Eqs. 17.63 and 17.64 have been used to split up the integral over T. We will also assume that the hard-sphere collision cross section σ is energy-independent; thus $k/\sigma N$ is a constant. To simplify the analysis, we introduce the following dimensionless energy variable:

$$y = \frac{E}{2E_d} \qquad (17.82)$$

and Eq. 17.81 is transformed to

$$\nu = \frac{1}{y} + \frac{2}{y}\int_1^y \nu(y')\, dy' - A\, y^{1/2}\frac{d\nu}{dy} \qquad (17.83)$$

where

$$A = \frac{k}{\sigma N\,(2E_d)^{1/2}} \qquad (17.84)$$

is a dimensionless constant. If A = 0, the Kinchin–Pease solution $\nu = y$ (see Eq. 17.68) is recovered. If A is small compared to unity, electronic stopping only slightly perturbs the basic Kinchin–Pease result. Assuming this to be the case, the number of displacements can be written as a power series in the perturbation parameter A:

$$\nu = y + f(y)\, A \ldots \qquad (17.85)$$

where the first term on the right is the solution for A = 0, and f(y) is a function to be determined by insertion of Eq. 17.85 into the integral equation, Eq. 17.83, which yields

$$f(y) = \frac{2}{y}\int_1^y f(y')\, dy' - y^{1/2} \qquad (17.86)$$

The solution of this equation can be obtained by differentiating, solving the differential equation, and determining the constant of integration by substitution into Eq. 17.86. In this way we find

$$f(y) = -4y + 3\, y^{1/2} \qquad (17.87)$$

If we restrict attention to high PKA energies ($E \gg E_d$), then $y \gg 1$, and the second term on the right in Eq. 17.87 can be dropped. Substituting $-4y$ for f(y) in Eq. 17.85 gives

$$\nu = y(1 - 4A) \qquad (17.88)$$

or

$$\nu(E) = \left[1 - \frac{4k}{\sigma N\,(2E_d)^{1/2}}\right]\left(\frac{E}{2E_d}\right) \quad (\text{for } E \gg E_d) \qquad (17.89)$$

Note that the validity of Eq. 17.89 is not subject to an upper limit on E, as is the case for Eq. 17.68. When electronic stopping is properly accounted for in the basic integral equation, the entire concept of a definite energy E_c separating regimes of electronic energy loss from atomic collisions can be jettisoned.

To assess the importance of electronic stopping on displacement production by energetic primary knock-ons, consider iron (Z = 26), for which k = 0.21 $eV^{1/2}$-Å (Eq. 17.53) and N = 0.085 $Å^{-3}$. We take E_d = 25 eV, and, for illustrative purposes, set $\sigma = 2Å^2$. With these values the coefficient of $E/2E_d$ in Eq. 17.89 is 0.3, or electronic energy losses have reduced the displacement efficiency of the PKA by 70%.

The sensitivity of the above calculation to the choice of the hard-sphere cross section suggests that the model should be entirely purged of hard-sphere characteristics and that realistic energy-transfer cross sections must be employed if reliable predictions are to be obtained. The complete calculation of Lindhard[17], as a matter of fact, used $\sigma_a(E,T_a)$ based on the Thomas–Fermi potential function rather than on the hard-sphere result.

Lindhard noted that the parameter $\nu(E)$ in Eq. 17.80 need not be interpreted solely as the number of displacements produced by a PKA. Rather, the integral equation is valid for a number of other radiation-damage effects, such as the number of ion pairs in a gas or the number of electron–hole pairs in a semiconductor. In the original analysis,[17] $\nu(E)$ was actually taken to be that part of the original PKA energy which is transferred to the atoms of the lattice (rather than to the electrons) during slowing down. The ratio of Lindhard's $\nu(E)$ to E is the fraction of the cascade energy transformed into atomic motion, which may be denoted by $\xi(E)$. Strictly speaking, Lindhard's application of Eq. 17.80 is not a displacement theory because it does not incorporate the displacement threshold restrictions at low energies, which are contained in Eqs. 17.63 and 17.64.* Lindhard's analysis has become known as the *energy-partitioning theory*.

Lindhard's energy-partitioning results can be used to predict displacements, however. For sufficiently high PKA energies, the number of displaced atoms is proportional to the original PKA energy (e.g., see Eq. 17.68 for an example of this proportionality in the simple Kinchin–Pease theory). Therefore, Lindhard's $\xi(E)$ can be used as a correction factor to the simple theory, and the number of displaced atoms is given by

$$\nu(E) = \xi(E)\left(\frac{E}{2E_d}\right) \qquad (17.90)$$

Lindhard's numerical solution of Eq. 17.80, using $(dE/dx)_e$ given by Eq. 17.52 and $\sigma_a(E,T_a)$ determined from an interaction potential based on the Thomas–Fermi model of the atom, can be expressed in the analytical form by

$$\xi(E) = \frac{1}{1 + 0.13(3.4\epsilon^{1/6} + 0.4\epsilon^{3/4} + \epsilon)} \qquad (17.91)$$

where ϵ is a reduced PKA energy:

$$\epsilon = \frac{E}{(2Z^2 e^2/a)} \qquad (17.92)$$

and a is the screening radius of Eq. 17.35 with $\lambda = 0.88$ and $Z_1 = Z_2$:

$$a = \frac{0.88 a_B}{Z^{1/3}} \qquad (17.93)$$

*When only energy transfer to, and not displacement of, lattice atoms is considered, the notion of a displacement energy E_d does not enter the calculation at all. Hence $\nu(E)$ increases continuously from E = 0, and the lower limit on the integral in Eq. 17.80 is kept as it is written.

Figure 17.11 shows the damage efficiency function ξ for various elements (i.e., for different values of Z). The dashed line represents the locus of the step-function ionization cutoff energies (E_c) employed in the Kinchin–Pease theory.

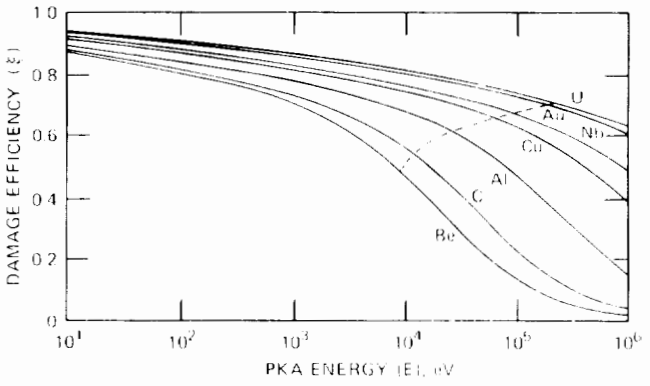

Fig. 17.11 Fraction of PKA energy deposited in the solid in the form of atomic collisions with lattice atoms (also used as the damage efficiency of the PKA). Solid lines are based on Lindhard's energy partitioning theory.[17] The dashed line gives the ionization cutoff for use in the Kinchin–Pease model. (E_c is read from the abscissa below the point at which the dashed line intersects the solid line for the particular elements.) (After Ref. 8.)

17.8 FOCUSING AND CHANNELING

The simple cascade analysis, even when modified to account for a realistic energy-transfer cross section or for electron excitation losses during slowing down, implicitly assumes that the solid consists of a random array of atoms. However, when the cascade is considered to occur in the ordered structure of a crystalline solid, two important phenomena appear: *Focusing* refers to the transfer of energy and atoms by nearly head-on collisions along a row of atoms and *channeling* is the complementary process whereby atoms move long distances in the solid along open directions in the crystal structure. In this case the moving atom is kept in its channel by glancing collisions with the atomic rows that serve as walls. Focusing and channeling affect both the number and configuration of displaced atoms in a cascade. First, atoms moving along the crystallographic direction favorable to either focusing or channeling lose energy only by glancing collisions with the atoms ringing the axis of motion. The energy transfer in these collisions is well below E_d, with the result that more energy is dissipated in subthreshold collisions than is predicted by the cascade theory reviewed in the preceding section [i.e., the number $\nu(E)$ is smaller when the crystal effects are considered than when the PKA enters a random array of atoms]. Second, the focused or channeled atoms are able to move much larger distances before coming to rest than ordinary knock-ons. In fact, the former may constitute the lion's share of the displaced atoms that escape recombination with the vacancies which are also produced in the cascade. As such, displaced atoms that have been created by focusing or channeling mechanisms contribute disproportionately to the radiation-produced interstitials that control radiation effects, such as diffusion-enhanced creep and void growth.

17.8.1 Focusing

The phenomenon of focusing can be seen in the calculations of the displacement threshold energies discussed in Sec. 17.6. When such calculations are made for various initial knock-on directions in the lattice (Fig. 17.7), we find that E_d is particularly small for certain low index directions in the crystal. For the fcc structure, for example, Fig. 17.7 shows that the ⟨100⟩ and ⟨110⟩ directions permit displacement to take place at the lowest energy transfer of any other lattice direction. This result at first seems somewhat unexpected, since in these directions the knock-on encounters a densely packed row of atoms rather than an open space with an interstitial site following it. The open configuration would be expected to permit displacement most easily. When directed along the ⟨100⟩ or ⟨110⟩ atomic rows in the fcc structure, the mechanism of knock-on penetration in the solid is very different from the way in which knock-ons initially headed in a more or less random direction achieve displacement. Along the closely packed directions, the knock-on hits a line of atoms head-on, and displacement can occur by the knock-on striking and replacing the nearest lattice atom along the row. The latter then collides with the next atom in a similar manner and replaces it. In this manner the well-known billiard-ball phenomenon in which a direct hit on the lead ball transfers the impact to the last ball in the line takes place. The last ball goes off with essentially the same energy with which the lead ball was hit. Such a linear collision chain can occur easily along the ⟨100⟩ and ⟨110⟩ directions in the fcc lattice (Fig. 17.6).

If a precise head-on collision were required to produce a linear collision chain, the phenomenon would be of no significance since the probability of its occurrence would be very small. The direction of a primary knock-on is random; so focusing must be possible for a sizable range of polar angles off the exact close-packed direction. Under certain circumstances the angle between the knock-on and the axis of the row of atoms is reduced in each successive collision. This property of the linear collision is responsible for the name "focused collision sequence."

The correlated collisions that occur in a linear chain of atoms can be analyzed easily if each atom is treated as a hard sphere of radius r_0. Suppose the distance between the atoms along a particular crystallographic row is denoted by D. Figure 17.12 shows three members of a row of atoms in which a sequence of nearly head-on collisions is propagating. The impact received by atom A_n from the atom to its left causes A_n to move off at an angle θ_n to the axis. The dashed circle shows A_n at the instant that the hard-sphere collision with atom A_{n+1} takes place. The impact transfers momentum to A_{n+1} in the direction along the radius terminating at the point of contact. The recoil angle θ_{n+1} of A_{n+1} can be related to the recoil angle of A_n by purely geometrical considerations. Applying the law of sines to the triangle (A_n, A_n', A_{n+1}) gives

$$\frac{\sin(\pi - \theta_n - \theta_{n+1})}{\sin \theta_n} = \frac{D}{2r_0}$$

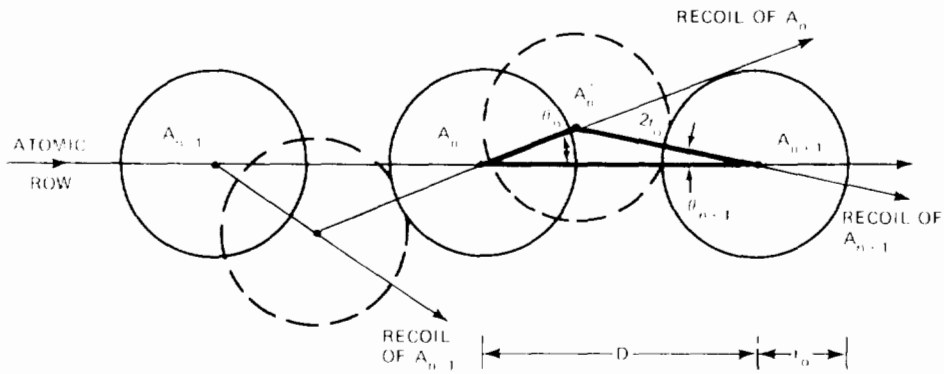

Fig. 17.12 The focused-collision sequence.

which, for small angles, reduces to

$$\frac{\theta_{n+1}}{\theta_n} = \frac{D}{2r_0} - 1$$

This relation is a first-order homogeneous finite-difference equation, the solution of which can be found by inspection to be

$$\theta_n = \left(\frac{D}{2r_0} - 1\right)^n \theta_0 \qquad (17.94)$$

where θ_0 is the angle that the primary knock-on makes with the crystallographic direction of the atomic row.

If $D > 4r_0$, the coefficient of θ_0 in Eq. 17.94 is larger than unity, and θ_n is larger than θ_0; thus the recoil angle becomes larger with each collision, and defocusing occurs. However, if $D < 4r_0$ (which is the situation depicted in Fig. 17.12), θ_n decreases with increasing n, and the collisions become more head-on in character. In this case the collision sequence is said to be focused. The criterion for focusing to just occur is $D = 4r_0$.

The focusing condition derived above is strictly geometric in origin since it relates the separation distance D to the radius r_0 of the hard spheres comprising the line of atoms. However, some degree of realism can be injected into the analysis by considering the radius r_0 to depend on the energy of the collision according to the equivalent hard-sphere model (Sec. 17.4). For the Born–Mayer potential function, which is appropriate to the low energies where focusing is important, r_0 depends on energy according to Eq. 17.41. We may determine the energy E_f at which focusing is just possible by eliminating $r_0(E)$ between Eq. 17.41 and the geometric focusing requirement, $D = 4r_0(E)$, which leads to

$$E < E_f = 2A \exp(-D/2\rho) \qquad (17.95)$$

If the energy of the initial collision is greater than E_f, focusing is impossible.

In the fcc structure, D is $2^{1/2} a_0$, a_0, and $a_0/2^{1/2}$ for the ⟨111⟩, ⟨100⟩, and ⟨110⟩ directions, respectively (a_0 is the lattice parameter). Thus focusing should occur most easily (i.e., E_f is the largest) along the close-packed ⟨110⟩ direction in metals with this crystal form. The focusing energy, E_f, also depends on the parameters A and ρ of the Born–Mayer potential. When these parameters are estimated for a variety of metals, E_f for any direction increases rapidly with the mass of the element. For example, $E_f\langle 110\rangle$ is about 80 eV in copper (using Eq. 17.95 and the Born–Mayer function shown in Fig. 17.5). For gold, it is about 600 eV. In both cases, however, the maximum energy at which focusing can occur (E_f) is small compared to typical PKA energies; thus focusing is important only in low-energy cascades or at the very end of a high-energy cascade.

Equation 17.94 states only the condition for which the recoil angle of the struck atom, θ_n, is reduced by successive collisions. It does not set any limit on the magnitude of the initial angle θ_0 at which focusing is possible. The maximum angle at which focusing just occurs, θ_0^f, for a PKA of energy $E < E_f$ can be determined by examining the situation in which the dashed circles in Fig. 17.12 are tangent to the solid circles. In this case all angles along the chain are equal to the initial angle θ_0. The triangle (A_n, A'_n, A_{n+1}) is isosceles, and the critical angle for focusing is determined by

$$\begin{aligned}\cos\theta_0^f &\sim 1 - \frac{1}{2}(\theta_0^f)^2 \\ &= \frac{D/2}{2r_0(E)} \\ &= \frac{D}{2\rho \ln(2A/E)} \\ &= \frac{\ln(2A/E_f)}{\ln(2A/E)}\end{aligned} \qquad (17.96)$$

where $r_0(E)$ has been expressed by Eq. 17.41 and Eq. 17.95 has been used to obtain the last form of the critical-angle formula.

The condition for focusing can be expressed by either of two quantities: (1) Eq. 17.95 gives the energy E_f for which focusing occurs for a head-on PKA collision ($\theta_0 = 0$) and (2) Eq. 17.96 gives the maximum angular deviation from a head-on collision, θ_0^f, at which a PKA of energy E can initiate a focused collision sequence. In this case E must be less than E_f.

Equation 17.96 can be used to obtain an important parameter that governs the reduction in the number of displaced atoms produced in a cascade owing to focused collisions. If any member of the cascade is produced in a collision that sends the struck atom within an angle θ_0^f to an atomic row, a focused collision sequence results, and the energy of the recoil is dissipated without making additional

displacements. In an ordinary displacement collision, the struck atom moves off its lattice site in a random direction. The probability that the initial direction of the struck atom is within a cone of apex angle θ_0 about an atomic row is, for small angles, given in spherical geometry by $(\theta_0)^2/2$. If we use the critical angle θ_0^f given by Eq. 17.96, the probability that a struck atom of energy E starts a focused collision sequence is

$$P_f(E) = \frac{1}{4}\{\theta_0^f(E)\}^2$$
$$= \frac{1}{2}\left[1 - \frac{\ln(2A/E_f)}{\ln(2A/E)}\right]$$
$$= \frac{1}{2}\frac{\ln(E/E_f)}{\ln(E_f/2A) + \ln(E/E_f)}$$

Since $E_f/2A \gg 1$ but E/E_f is of order unity (unless E becomes very small), the second term in the denominator can be neglected, and we obtain

$$P_f(E) = \frac{1}{2}\frac{\ln(E/E_f)}{\ln(E_f/2A)} \quad (\text{for } E < E_f)$$
$$= 0 \quad (\text{for } E > E_f) \qquad (17.97)$$

17.8.2 Dynamic Crowdions

Successive head-on collisions along a line of hard-sphere atoms transport the initial kinetic energy of the initiating atom down the row. In addition, the entire row of atoms can be displaced by one lattice site in the direction of the travelling energy pulse provided the following condition is met: With reference to Fig. 17.12, if the A_n' is beyond the midpoint of the initial separation between A_n and A_{n+1}, then A_n will fall into the site vacated by the recoiling A_{n+1}. This replacement event is repeated along the line of atoms, with the net result that a vacant site appears at the starting location of the collision sequence and an interstitial is lodged in the solid somewhere far down the line of atoms where, by some other mechanism, the chain of head-on collisions is terminated. This long-range transport of a single atom is known as a *focused replacement* or a *dynamic crowdion.**

If we adhere to the hard-sphere model that was used previously to calculate the energy focusing criteria E_f or $P_f(E)$, we would find that the focused replacement is impossible; focusing (with or without replacement) occurs only when $D < 4r_0$; yet in a head-on collision with this restriction, the center of the first atom at the point of impact (A_n' in Fig. 17.12) is always closer to A_n than to A_{n+1}. Consequently, if we are to describe the focused replacement process, the hard-sphere assumption must be modified earlier in the analysis than it was in the argument leading to prediction of the focusing criterion. In the latter case the possibility of focusing was decided by purely geometric arguments based on the relative magnitudes of D and r_0, and the real interatomic potential was introduced only at the end by allowing r_0 to depend on E according to the equivalent hard-sphere model. In the present case, however, we must permit the interaction to begin before the distance of closest approach is reached and the relative velocity of the colliding particles vanishes. In this way atom A_{n+1} is induced to move as soon as atom A_n starts to move, and, consequently, A_{n+1} is to the right of its initial position when the turnaround occurs.

It is sufficient to analyze the focused replacement process in terms of the head-on collision shown in Fig. 17.13(a). As the collision proceeds, the distance x between A_n and A_{n+1} decreases continuously as shown in Fig. 17.13(b). At any point during the collision, the relative speed of the two atoms, g, is related to the interaction energy V(x) according to Eqs. 17.15 and 17.16:

$$\frac{1}{2}\mu g^2 + V(x) = \frac{1}{2}\mu g_0^2 \qquad (17.98)$$

where the reduced mass μ is equal to M/2 since the colliding atoms are identical and the initial relative speed, g_0, is equal to the initial speed of atom A_n, v_{10}. Equation 17.98 also assumes that the interaction energy at the initial separation, V(D), is small compared with the initial relative kinetic energy, $\mu g_0^2/2$. The time rate of change of the separation is equal to the relative speed

$$\frac{dx}{dt} = -g \qquad (17.99)$$

Since the curve shown in Fig. 17.13(b) is symmetric about the midpoint, the collision time t_c is twice the time needed to reach the distance of closest approach, or

$$t_c = -2\int_D^{x_m}\frac{dx}{g} = -2\int_{V(D)}^{V(x_m)}\frac{dV}{g(dV/dx)}$$

where x_m is the distance of closest approach in the head-on collision. Note that V(D) is not set equal to zero in the above integral. If we evaluate dV/dx from the Born–Mayer potential function of Eq. 17.32 and solve Eq. 17.98 for g as a function of V (using the conditions $\mu = M/2$ and $\mu g_0^2/2 = E/2$, where E is the kinetic energy received by atom A_n in its previous collision), t_c becomes

$$t_c = \rho\left(\frac{2M}{E}\right)^{1/2}\int_{V(D)}^{E/2}\frac{dV}{V(1-2V/E)^{1/2}} = 2\rho\left(\frac{2M}{E}\right)^{1/2} \times \tanh^{-1}\left[1 - \frac{2V(D)}{E}\right]^{1/2}$$

where the definition of the equivalent hard-sphere radius given by Eq. 17.17 has been used for the upper integration limit. For $V(D)/E \ll 1$, the above formula can be simplified to yield

$$t_c = \rho\left(\frac{2M}{E}\right)^{1/2}\ln\left[\frac{2E}{V(D)}\right] \qquad (17.100)$$

The speed of the center of mass of the two-particle system is $v_{10}/2 = (E/2M)^{1/2}$. The distance moved by the center of mass during the collision time t_c is $t_c(E/2M)^{1/2}$. If this distance is larger than one-half the initial separation, D/2, then atom A_n will end up to the right of the halfway point between the atoms before collision. When this situation occurs, atom A_n enters the lattice site vacated by atom

*The term crowdion refers to an extra atom squeezed into a line of atoms. It is a type of interstitial similar to the split interstitials shown in Fig. 6.4. The dynamic crowdion is a crowdion in motion.

A_{n+1} instead of returning to its own lattice position. Replacement has occurred. According to the above arguments, focused replacement is possible when the energy being transported in the collision chain satisfies

$$E > E_r = \frac{1}{2} A \exp\left(\frac{-D}{-2\rho}\right) = \frac{1}{4} E_f \qquad (17.101)$$

Regardless of whether or not replacement occurs, no focusing is possible if the energy is larger than E_f. Thus, dynamic crowdions can be created by a knock-on with energy between $E_f/4$ and E_f but not with energies outside this range. In metals of interest in reactor technology (primarily iron), the focusing energy E_f in the close-packed direction is ~100 eV. Therefore, the replacement energy $E_r = E_f/4$ is probably somewhat smaller than the displacement energy E_d, and the formation of a dynamic crowdion has a slightly lower threshold than the production of a random displaced atom. This conclusion is consistent with the displacement thresholds shown in Fig. 17.7, which indicate that the ⟨100⟩ direction, for which $D = a_o$, has a smaller replacement threshold than does the ⟨110⟩ direction, where $D = a_o/2^{1/2}$. On the basis of Eq. 17.101, one would expect that the replacement threshold in the ⟨111⟩ direction should be even smaller since here $D = 2^{1/2} a_o$. In this case, however, displacement is governed by the energy required to force the struck atom through the triangle of atoms along the ⟨111⟩ direction and not by the energy needed to generate a dynamic crowdion. Hence, Eq. 17.101 does not apply to the ⟨111⟩ direction in the fcc structure.

Thus far the analysis of the dynamic crowdion has been restricted to the behavior of the atomic row along which both energy and atoms are transported. In this idealized model the collision sequence continues indefinitely since there is no mechanism for removing energy from the chain. Two effects appear when the interaction of the neighboring rows of atoms with the row along which a focused collision is occurring is taken into account.

First, the neighboring atoms, by their repulsion of a moving atom that approaches more closely than the equilibrium separation, act as a lens and aid in the focusing process (i.e., they tend to reduce the angle θ_n on successive collisions to a greater extent than predicted by simple hard-sphere mechanics along the chain). The net result of this process, which is called *assisted focusing*, is to increase the critical energy E_f at which a focused collision sequence is possible. Focusing is rendered more probable by the presence of the surrounding atomic rows (see Ref. 1 for a detailed discussion of assisted focusing).

Second, in addition to aiding the focusing process, the rings of atoms surrounding a focusing axis in the crystal provide the only means by which the energy of the collision sequence is dissipated. The energy loss results from glancing collisions between the atoms moving in the linear collision sequence and the atoms ringing this chain. This energy transfer occurs as a result of the decrease in the separation distance between an atom in the focused collision chain and its transverse nearest neighbors as the former moves off of its equilibrium position along the focusing axis. The increment of potential energy which results from the smaller separation between the moving atom in the chain and the neighboring atoms ringing the chain is lost to the energy pulse moving along the line (see problem 17.5 at the end of this chapter). This effect is augmented by vibration of the surrounding atoms transverse to the focusing direction, which increases with the temperature of the solid.

Figure 17.14 shows the number of collisions in a focused chain of initial energy E in room-temperature copper. The transport of energy along the focusing axis ends when interaction with the neighboring atoms has removed the entire initial energy of the knock-on that started the sequence. Focused replacement ceases when the energy left in the chain is reduced to $E_f/4$. Thus the length of the dynamic crowdion for initial knock-on energy E is the difference between the ordinate value corresponding to

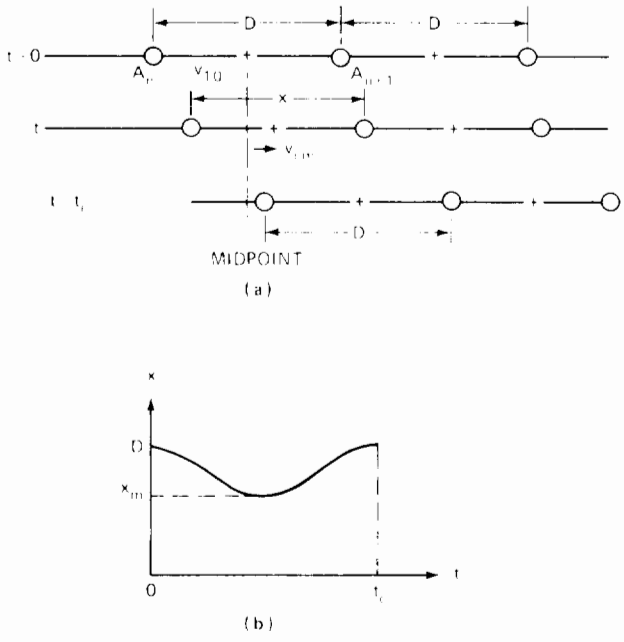

Fig. 17.13 Head-on collisions in a focused chain when the interaction potential acts continuously during the collision. (a) Atom positions during the collision initiated by the atom on the left. (b) Separation of atoms A_n and A_{n+1} during the collision.

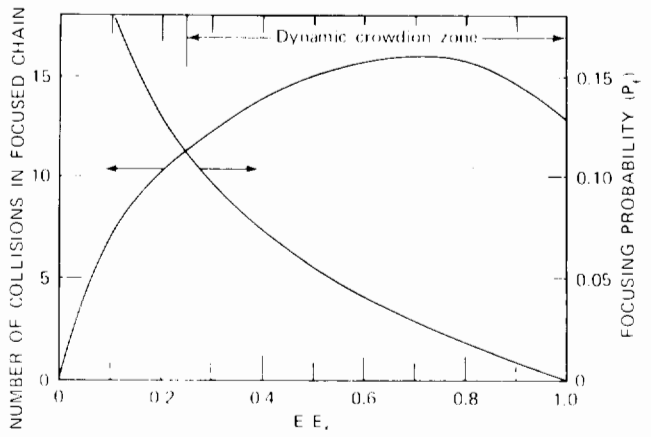

Fig. 17.14 Length and probability of the collision chain in a ⟨110⟩ collision sequence in copper at room temperature. (After Ref. 1.)

E/E_f and the ordinate value for $E/E_f = 1/4$. The length of the chain or of the dynamic crowdion decreases as the temperature increases due to the greater interference of displaced neighboring atoms with the collision sequence as the thermal vibration amplitude increases. The probability of forming a correlated collision sequence according to Eq. 17.97 is also shown in Fig. 17.14.

The presence of atoms of unequal mass in the atomic row also serves to dissipate energy from the collision chain. Consider a light atom sandwiched between two heavy atoms along the focusing axis. When struck, the light atom not only collides with the downstream heavy atom but may also rebound rapidly enough to re-collide with the upstream heavy atom from which it received the original impact. Such multiple collision events destroy the unidirectional nature of the energy pulse and result in substantial energy loss. This dissipation mechanism may be important in stainless steel, which contains substantial quantities of low-mass additives such as carbon and boron in addition to the transition metals iron, nickel, and chromium, which have not too different masses. A similar effect would be expected if a focusing axis intersected a lattice defect, such as a vacancy.

Extended lattice defects, such as a dislocation or a stacking fault (i.e., an interruption of the stacking sequence of the planes of a crystal), represent such large distortions of the crystal symmetry that they probably terminate the dynamic crowdion, which then becomes lodged in the solid as an interstitial atom. For a heavily deformed matrix with a dislocation density of 10^{12} cm^{-2}, for example, the average distance between dislocation lines is about 100 Å, or 40 atom separation distances in the ⟨110⟩ direction of the fcc lattice. This chain length is three times longer than the average number of collisions along the focusing axis when interaction with the atoms surrounding the focusing axis is responsible for energy dissipation (Fig. 17.14). Limitation of the length of a dynamic crowdion is most probably controlled by this intrinsic dissipation mechanism rather than by interaction with dislocations, especially at high temperature.

17.8.3 Channeling

Channeling refers to the long-distance displacement of an energetic knock-on down an open direction in the lattice. The walls of the passageway or channel consist of atomic rows. Figure 17.15 shows the ⟨110⟩ channel in the fcc structure, which is bounded by four close-packed ⟨110⟩ atomic rows. Atoms moving by the focusing or channeling mechanisms both prefer to do so in close-packed directions in the lattice. However, dynamic crowdions move in the close-packed rows, whereas channeled atoms move in between the close-packed rows.

The moving atom is kept in a channel by glancing collisions with the bordering atoms. If the atomic rows surrounding the channel are close packed, the discrete repulsive force between atoms, which is responsible for the channeling action, is smeared out, and the atom appears to be travelling in a long cylindrical tube. The equivalent radius of the channel, R_{ch}, can be determined by equating πR_{ch}^2 with the actual area of the open region between the surrounding atomic rows. The cross-sectional area of the ⟨110⟩ channel shown in Fig. 17.15, for example, is $a_o^2/8^{1/2}$; so $R_{ch} = 0.34a_o \sim 0.85$ Å.

If the amplitude of the lateral oscillations of the moving atom in the channel is small compared to R_{ch}, the effective potential well provided by the channel wall is approximately parabolic in the direction transverse to the channel axis. The interaction of the moving atom with the channel walls can be described by a harmonic channel potential of the form

$$V_{ch}(r) = \kappa r^2 \qquad (17.102)$$

where r is the lateral distance from the axis. The force constant, κ, depends on the potential function describing atom–atom repulsion and the channel dimensions R_{ch}. An

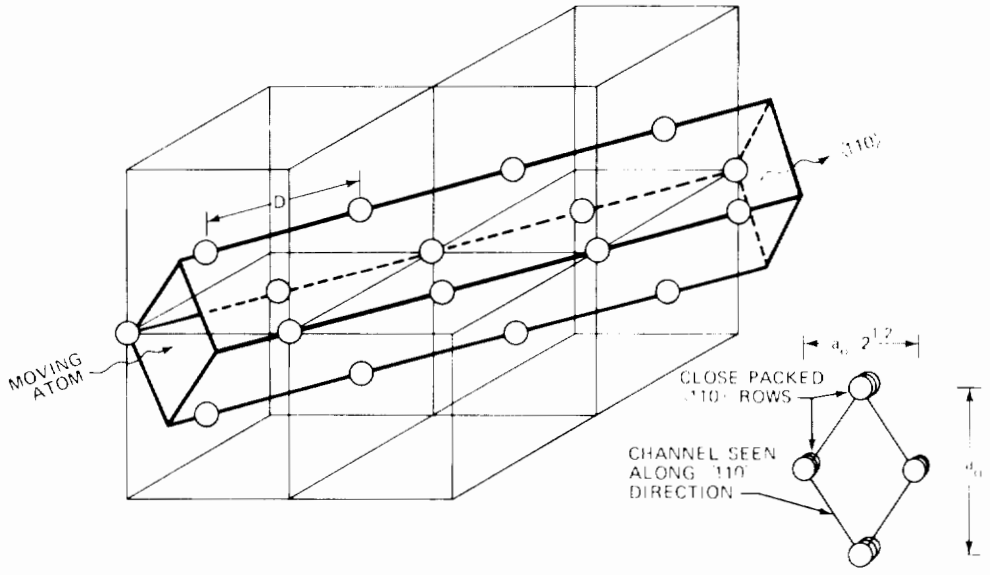

Fig. 17.15 The ⟨110⟩ channel in the fcc lattice.

approximate derivation of the force constant is given in Ref. 1. For the Born—Mayer function, for example, it is

$$\kappa = \frac{A}{D\rho}\left(\frac{2\pi R_{ch}}{\rho}\right)\exp\left(-\frac{R_{ch}}{\rho}\right) \qquad (17.103)$$

where D is the atomic spacing of the atoms in the rows forming the channel walls.

Analysis of the trajectory of the channeled atoms with the aid of the parabolic channel potential of Eq. 17.102 is straightforward. The moving atom enters into the channel with a velocity component along the axis (the z-direction) given by

$$v_{z0} = (2E/M)^{1/2}\cos\theta_0 \qquad (17.104)$$

where θ_0 is the off-axis angle at which the knock-on of energy E is injected into the channel. The axial velocity is gradually reduced by electron stopping.

The moving atom undergoes simple harmonic motion in the r-direction with a period τ given by

$$\tau = 2\pi\left(\frac{M}{2\kappa}\right)^{1/2} \qquad (17.105)$$

The initial wavelength of the oscillation is equal to $v_{z0}\tau$ for $\theta_0 = 0$, or to

$$\lambda = 2\pi\left(\frac{E}{\kappa}\right)^{1/2} \qquad (17.106)$$

The amplitude of the lateral oscillation is determined by the injection angle, θ_0, and the kinetic energy of the injected atom, E. The r-component of the atom velocity as it enters the channel is $(2E/M)^{1/2}\sin\theta_0 \sim (2E/M)^{1/2}\theta_0$. Or, the radial component of the entrance kinetic energy is $E\theta_0^2$, which is equal to the potential energy at the transverse amplitude, κr_{max}^2. Solving for r_{max} yields

$$r_{max} = \left(\frac{E}{\kappa}\right)^{1/2}\theta_0 \qquad (17.107)$$

and the trajectory of the channeled atom is

$$r = \theta_0\left(\frac{E}{\kappa}\right)^{1/2}\sin\left[\left(\frac{\kappa}{E}\right)^{1/2}z\right] \qquad (17.108)$$

A typical trajectory is shown in Fig. 17.16.

Just as in the case of focusing, there is a critical angle beyond which channeling cannot occur. In the harmonic approximation, θ_0^{max} is obtained by requiring that the transverse amplitude r_{max} be less than R_{ch}, which leads to

$$\theta_0^{max} = \left(\frac{\kappa R_{ch}^2}{E}\right)^{1/2} \qquad (17.109)$$

Equation 17.109 is the analog of the critical-angle formula derived for focusing (Eq. 17.96). However, the former cannot be used to determine a channeling probability, P_{ch}, in the way that the focusing probability, P_f, given by Eq. 17.97 was obtained from Eq. 17.96. The reason is that for channeling to begin an energetic knock-on must be driven into the open space offered by the channel. For the very reason that a channel is open, there are no normal lattice atoms near the channel axis to act as the channeled atom. Instead, channeling probably starts with an impact on one of the atoms in the row forming the channel walls. If this atom leaves its lattice position at a small angle with respect to the axis, it may begin to channel. Equation 17.109 was derived for an atom entering the channel at $r = 0$ and cannot be applied to a knock-on entering at $r = R_{ch}$. Although no analytical expression for the channeling probability is available, computer simulations of radiation damage indicate that P_{ch} is between 1 and 10%. It is usually assumed to be independent of knock-on energy.

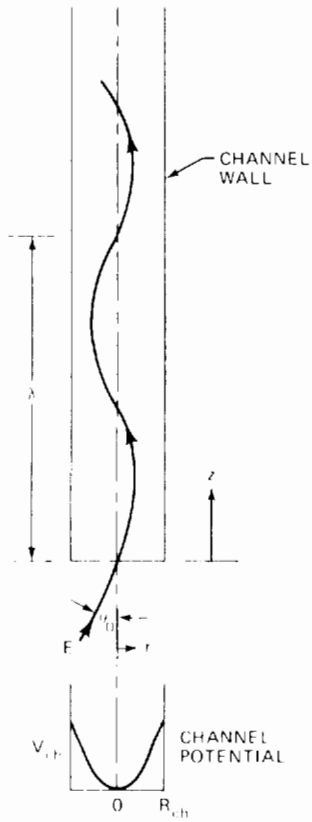

Fig. 17.16 Typical trajectory of channeled atom.

Contrary to the phenomenon of focusing, there is no upper limit to the knock-on energy at which channeling is possible; the maximum allowable injection angle simply becomes smaller as the energy increases. However, there is a minimum energy below which the oscillatory motion is terminated by a violent collision with the channel wall. Equation 17.106 shows that the wavelength decreases as the energy of the channeled atom decreases. When λ is of the order of a few atom spacings along the bounding rows, a large-angle collision becomes probable. The minimum channeling energy, E_{ch}, can be estimated by setting λ in Eq. 17.106 equal to 2D, which yields

$$E_{ch} = 0.1\kappa D^2 \qquad (17.110)$$

For copper, $E_{ch} = 300$ eV. The energy E_{ch} increases directly as κ. When available Born—Mayer parameters are used in Eq. 17.103, κ, and hence E_{ch}, are found to be larger for heavy elements than for light ones. Thus, channeling is a high-energy phenomenon of most significance in low-atomic-weight metals. Conversely, focusing is possible only at low energies and is more important in heavy elements than in light ones.